Invading viral DNA triggers dsRNA synthesis by RNA polymerase II to activate antiviral RNA interference in Drosophila

Isaque J.S. de Faria, Eric R.G.R. Aguiar, Roenick Proveti Olmo, Juliana Alves da Silva, Laurent Daeffler, Richard W. Carthew, Jean-Luc Imler, João T. Marques

Cell Reports

Article

Invading viral DNA triggers dsRNA synthesis by RNA polymerase II to activate antiviral RNA interference in *Drosophila*

Graphical abstract

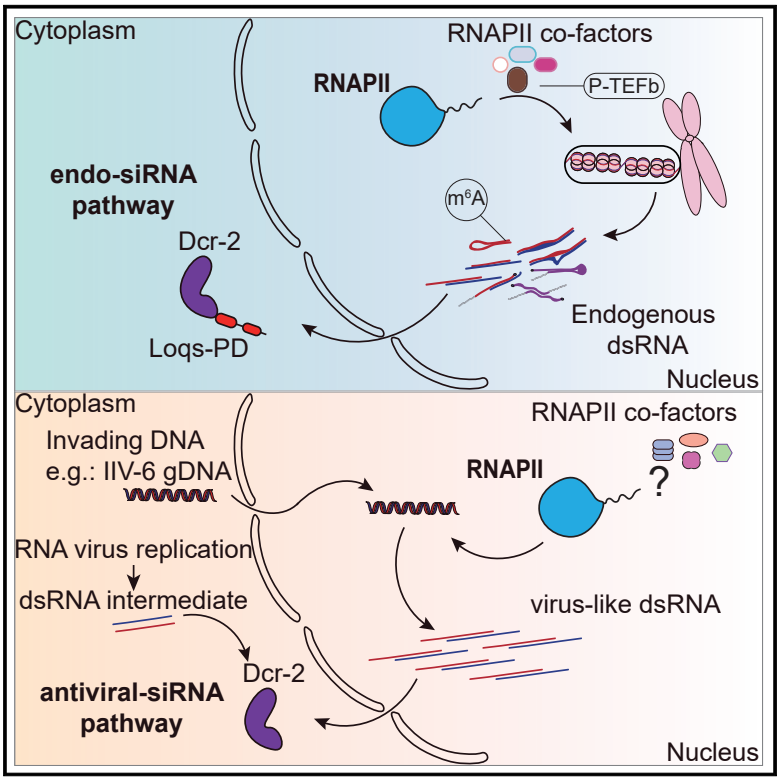

Highlights

- Invading DNA generates dsRNAs in *Drosophila* cells in the absence of viral proteins
- Host RNA polymerase II produces virus-derived dsRNAs from invading viral DNA
- dsRNA synthesis from viral DNA does not require canonical RNA polymerase II co-factors
- The siRNA pathway can discriminate viral dsRNAs produced by cellular RNA polymerase II

Authors

Isaque J.S. de Faria, Eric R.G.R. Aguiar, Roenick P. Olmo, ..., Richard W. Carthew, Jean-Luc Imler, João T. Marques

Correspondence

jtm@ufmg.br

In brief

dsRNA is essential to mount antiviral defenses in metazoans, but its origin during DNA virus infections is complex. de Faria et al. report that, in *Drosophila*, a non-canonical host RNA polymerase II complex synthesizes dsRNAs upon recognition of invading DNA, which fuels the activation of the antiviral siRNA pathway.

de Faria et al., 2022, Cell Reports *39*, 110976
June 21, 2022
https://doi.org/10.1016/j.celrep.2022.110976

CellPress

Cell Reports

CellPress
OPEN ACCESS

Article

Invading viral DNA triggers dsRNA synthesis by RNA polymerase II to activate antiviral RNA interference in *Drosophila*

Isaque J.S. de Faria,[1,2] Eric R.G.R. Aguiar,[1,3] Roenick P. Olmo,[1,2] Juliana Alves da Silva,[4] Laurent Daeffler,[2] Richard W. Carthew,[5,6] Jean-Luc Imler,[2] and João T. Marques[1,2,7,*]

[1]Department of Biochemistry and Immunology, Instituto de Ciências Biológicas, Universidade Federal de Minas Gerais, 31270-901 Belo Horizonte, Brazil

[2]Université de Strasbourg, CNRS UPR9022, INSERM U1257, 67084 Strasbourg, France

[3]Department of Biological Science (DCB), Center of Biotechnology and Genetics (CBG), Universidade Estadual de Santa Cruz (UESC), 45662-900 Ilhéus, Brazil

[4]Department of Morphology, Instituto de Ciências Biológicas, Universidade Federal de Minas Gerais, 31270-901 Belo Horizonte, Brazil

[5]Department of Molecular Biosciences, Northwestern University, Evanston, IL 60208, USA

[6]NSF Simons Center for Quantitative Biology, Northwestern University, Evanston, IL 60208, USA

[7]Lead contact

*Correspondence: jtm@ufmg.br

https://doi.org/10.1016/j.celrep.2022.110976

SUMMARY

dsRNA sensing triggers antiviral responses against RNA and DNA viruses in diverse eukaryotes. In *Drosophila*, *Invertebrate iridescent virus 6* (IIV-6), a large DNA virus, triggers production of small interfering RNAs (siRNAs) by the dsRNA sensor Dicer-2. Here, we show that host RNA polymerase II (RNAPII) bidirectionally transcribes specific AT-rich regions of the IIV-6 DNA genome to generate dsRNA. Both replicative and naked IIV-6 genomes trigger production of dsRNA in *Drosophila* cells, implying direct sensing of invading DNA. Loquacious-PD, a Dicer-2 co-factor essential for the biogenesis of endogenous siRNAs, is dispensable for processing of IIV-6-derived dsRNAs, which suggests that they are distinct. Consistent with this finding, inhibition of the RNAPII co-factor P-TEFb affects the synthesis of endogenous, but not virus-derived, dsRNA. Altogether, our results suggest that a non-canonical RNAPII complex recognizes invading viral DNA to synthesize virus-derived dsRNA, which activates the antiviral siRNA pathway in *Drosophila*.

INTRODUCTION

Sensing of virus-derived double-stranded RNA (dsRNA) is central to antiviral immunity in metazoans. There are a variety of pattern recognition receptors, referred to as dsRNA sensors, that play a role in the recognition and effector mechanisms during viral infection (de Faria et al., 2013). Viruses often produce dsRNA during their replication cycle, regardless of genome structure (Dewitte-orr and Mossman, 2010; Son et al., 2015; Weber et al., 2006). Although dsRNA is often referred to as a by-product of genome replication of RNA viruses, dsRNA is also commonly found in cells infected by DNA viruses (Son et al., 2015; Weber et al., 2006). These dsRNAs are often associated with transcription of convergent genes to produce complementary RNAs (Aloni, 1972; Boone et al., 1979; Burgess and Mohr, 2015; Duesberg and Colby, 1969; Jacobs and Langland, 1996; Jacquemont and Roizman, 1975; Kumar and Carmichael, 1998; Liu et al., 2015; Lucas and Ginsberg, 1972; Peacock et al., 1969; Weber et al., 2006). Indeed, this is facilitated by the fact that DNA viruses have highly compact genomes harboring short intergenic regions (IRs) with inefficient termination signals on viral open reading frames (ORFs) (Jacobs and Langland, 1996; Kumar and Carmichael, 1998). Alternatively, host cells can generate dsRNAs upon recognition of viral DNA. In mammals, RNA polymerase III (RNAPIII) senses and converts cytoplasmic AT-rich dsDNA into stimulatory dsRNA species to activate the antiviral RNA helicase RIG-I (Ablasser et al., 2009; Chiu et al., 2009). Sensing of dsRNA by the Toll receptor TLR3 plays an important role in the control of herpesvirus, a large dsDNA virus, in mammals (Tabeta et al., 2004; Zhang et al., 2007). These data reinforce the idea that dsRNA recognition plays a broad role in the antiviral defense. Accordingly, DNA viruses commonly encode mechanisms that target dsRNA sensors through degradation, decoys, and pseudo-substrates (Dewitte-orr and Mossman, 2010).

Invertebrates heavily depend on the small interfering RNA (siRNA) pathway for antiviral defense against DNA and RNA viruses, which is mediated by dsRNA sensing (Bronkhorst et al., 2012; Jayachandran et al., 2012; Kemp et al., 2013; Marques and Imler, 2016; Sabin et al., 2013; Webster et al., 2015). In *Drosophila*, the RNA helicase Dicer-2 (Dcr-2) senses long dsRNA that is processed into 21-nt-long siRNAs, which are loaded onto the endonuclease Argonaute 2 (AGO2) by a complex consisting of Dcr-2, R2D2, and TAF11 (Deddouche et al.,

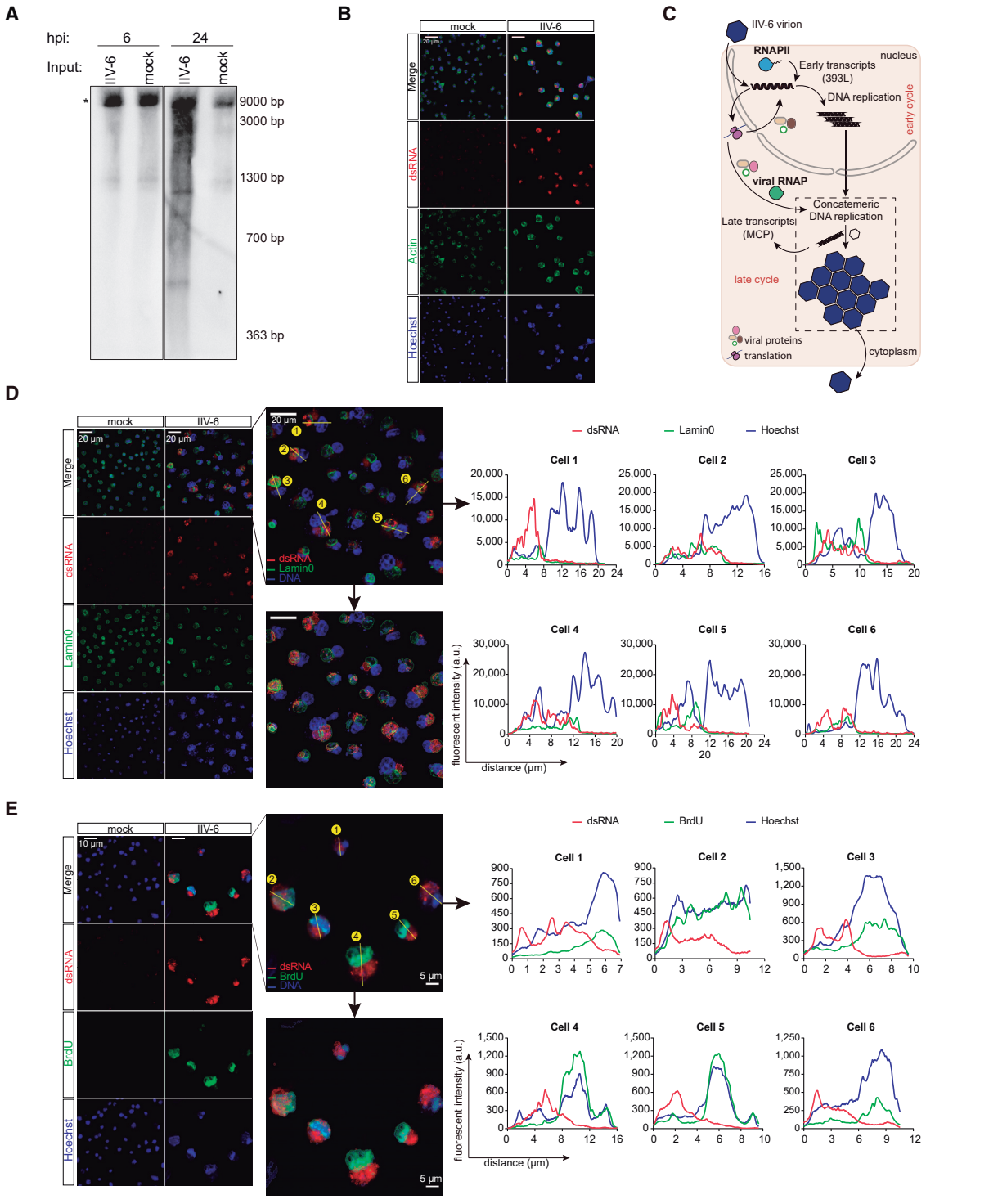

Figure 1. IIV-6 generates dsRNA upon infection of *Drosophila* cells

(A) Detection of dsRNA by immunoblotting of total RNAs from IIV-6- or mock-infected S2 cells at different times post infection. *Non-specific bands. hpi, hours post infection.

(B) Immunofluorescence (IFA) of dsRNA in IIV-6- and mock-infected S2 cells (Hoechst/DNA, blue; dsRNA, red; phalloidin/actin, green). Scale bars: 20 μm.

(C) Cartoon depicting crucial steps in iridovirus replication. The iridovirus genomic DNA (gDNA) invades the nucleus and uses host RNA polymerase II (RNAPII) to transcribe early genes (e.g., 393L) that coordinate DNA replication and synthesis of the viral RNA polymerase. Viral gDNA initially replicates in the nucleus and then is translocated into the cytoplasm for final replication and late transcription (e.g., MCP) to produce and release viral particles.

(legend continued on next page)

2008; Galiana-Arnoux et al., 2006; Lee et al., 2004; Liang et al., 2015; Liu et al., 2003). AGO2 is the core of the RNA-induced silencing complex (RISC), which targets and degrades viral RNA transcripts by complementarity, thus restricting viral infections (Hammond et al., 2001; Schwarz et al., 2003; van Rij et al., 2006; Wang et al., 2006). This defense mechanism functions against not only RNA viruses, but also DNA viruses, including *Invertebrate iridescent virus 6* (IIV-6), a member of the nucleocytoplasmic large dsDNA viruses (NCLDVs) (Bronkhorst et al., 2012; Kemp et al., 2013). The importance of the siRNA pathway for defense against IIV-6 is highlighted by the facts that *Dcr-2* and *AGO2* mutant flies are more susceptible to infection and the virus encodes an inhibitor of RISC (Bronkhorst et al., 2012, 2019; Kemp et al., 2013). In infected flies, IIV-6-derived siRNAs are generated symmetrically from both strands of the genome, suggesting they are produced from long dsRNA precursors by Dcr-2 processing (Bronkhorst et al., 2012; Kemp et al., 2013). However, unlike most RNA viruses, IIV-6-derived siRNAs are not uniformly generated across the virus genome, and the origin and biogenesis of dsRNA precursors remain unclear.

Although a hallmark of virus infection, dsRNA also exists in non-infected cells and is encoded by the host cell genome (Dhir et al., 2018; Ilyin et al., 1980; Jelinek and Darnell, 1972). *Drosophila* endogenous dsRNAs arise from structured loci, *cis* natural antisense transcripts (cis-NATs), and transposable elements (TEs), and are thereafter converted into siRNAs (Chung et al., 2008; Czech et al., 2008; Ghildiyal et al., 2008; Kawamura et al., 2008; Okamura et al., 2008). Dcr-2 discriminates dsRNA origins using Loquacious-PD (Loqs-PD), a dsRNA binding protein (dsRBP) required for dicing endogenous dsRNAs but not dsRNAs from cytoplasmic RNA viruses (Han et al., 2011b; Marques et al., 2013; Zhou et al., 2009). It remains unclear how Dcr-2/Loqs-PD can discriminate between viral and endogenous dsRNA and whether this also applies to molecules derived from DNA viruses.

Here, we focus on the origin and recognition of dsRNAs generated in response to IIV-6 infection in *Drosophila*. Our results suggest that sensing of invading DNA promotes non-canonical RNAPII transcription to generate dsRNA and trigger antiviral RNAi.

RESULTS

dsRNA accumulates in IIV-6-infected cells

In fruit flies infected with IIV-6, the presence of siRNAs suggests that virus-derived dsRNA is produced, although this has not been formally shown. We infected *Drosophila* S2 cells with IIV-6 and observed accumulation of dsRNA by immunoblotting at 24 h post infection (hpi) (Figure 1A). dsRNA was heterogenous in size and not as abundant as in cells infected with the RNA virus *Drosophila* C virus (DCV), known to generate large amounts of dsRNA (Monsion et al., 2018) (Figure S1A). By immunofluorescence, we also observed the accumulation of dsRNA in infected cells (Figure 1B). Interestingly, iridoviruses have a complex replication cycle involving an early step in the nucleus and a later more robust stage in the cytoplasm where the viral factory is formed (Figure 1C) (Chinchar et al., 2011). Using an antibody against *Drosophila* Lamin, which labels the inner nuclear membrane, we observed that most dsRNAs accumulated in the nucleus of infected cells (Figures 1D and S1B). Indeed, dsRNA signals were mostly excluded from cytoplasmic factories containing replicating viral DNA labeled with bromodeoxyuridine (BrdU) (Figures 1E and S1C). These data suggest that dsRNA is produced in the nucleus of IIV-6-infected cells, separate from late viral factories that are in the cytoplasm.

Mapping dsRNA precursors on the IIV-6 genome based on siRNA coverage

To address the origin of the IIV-6-derived dsRNAs, we analyzed four independent small RNA-sequencing (sRNA-seq) datasets from cells and flies infected with IIV-6 (Figure 2A). There was a remarkably consistent pattern of siRNA coverage along the viral genome (Figure 2A, top left). The striking conservation of the siRNA coverage suggests that the production of dsRNA precursors is biased toward specific regions of the viral genome.

To better define regions that generate dsRNA precursors, we selected the most covered base positions in the IIV-6 genome based on sRNA read density using a 95% confidence interval (Figure 2A). A total of 3,006 bases were shared among the four independent datasets, which we considered to be hotspots for siRNA production in the IIV-6 genome (Figure 2A, top right). The siRNA hotspots mapped to open reading frames (ORFs) and intergenic regions in the IIV-6 genome, with continuous coverage of siRNA reads between adjacent regions, indicating that dsRNA precursors were not restricted to gene units. Based on this observation, instead of analyzing individual ORFs, we defined 14 genomic regions with continuous and homogeneous siRNA read coverage that contained all 3,006 hotspots (see STAR Methods for details), hereafter named hotspot-associated regions (Figures 2A and 2B). These were interspersed with large areas of the virus genome with poor siRNA coverage that we refer to as hotspot-depleted regions, also numbered from 1 through 14 (Figure 2B). The 14 hotspot-associated regions had a larger than expected contribution to the share of IIV-6-derived siRNAs (Figure 2B). Notably, hotspot-associated regions were significantly more AT rich than the rest of the genome, despite the low CG content of the IIV-6 genome as whole (Figure 2C). In addition, we identified an AT-rich sequence motif that is significantly enriched close to hotspot-associated regions compared with other motifs that are found throughout the viral genome (Figures S2A and S2B). These results indicate that specific

(D) dsRNA and Lamin0 labeling in IIV-6-infected S2 cells analyzed by IFA. Z-projected confocal images are shown on the left. Middle: cross-section analysis (top) and dsRNA (red), Lamin0 (green), and Hoechst/DNA (blue) areas (bottom). Right: cross-section quantification for individual cells depicted in the middle. Scale bars: 20 μm. a.u., arbitrary units.

(E) dsRNA and BrdU labeling in IIV-6-infected S2 cells analyzed by IFA. Z-projected confocal images are shown on left. Middle: cross-section analysis (top) and dsRNA (red), BrdU (green), and DNA (blue) areas (bottom). Right: cross-section quantification for individual cells depicted in the middle. Scale bars: 10 μm (left) and 5 μm (right). a.u., arbitrary units.

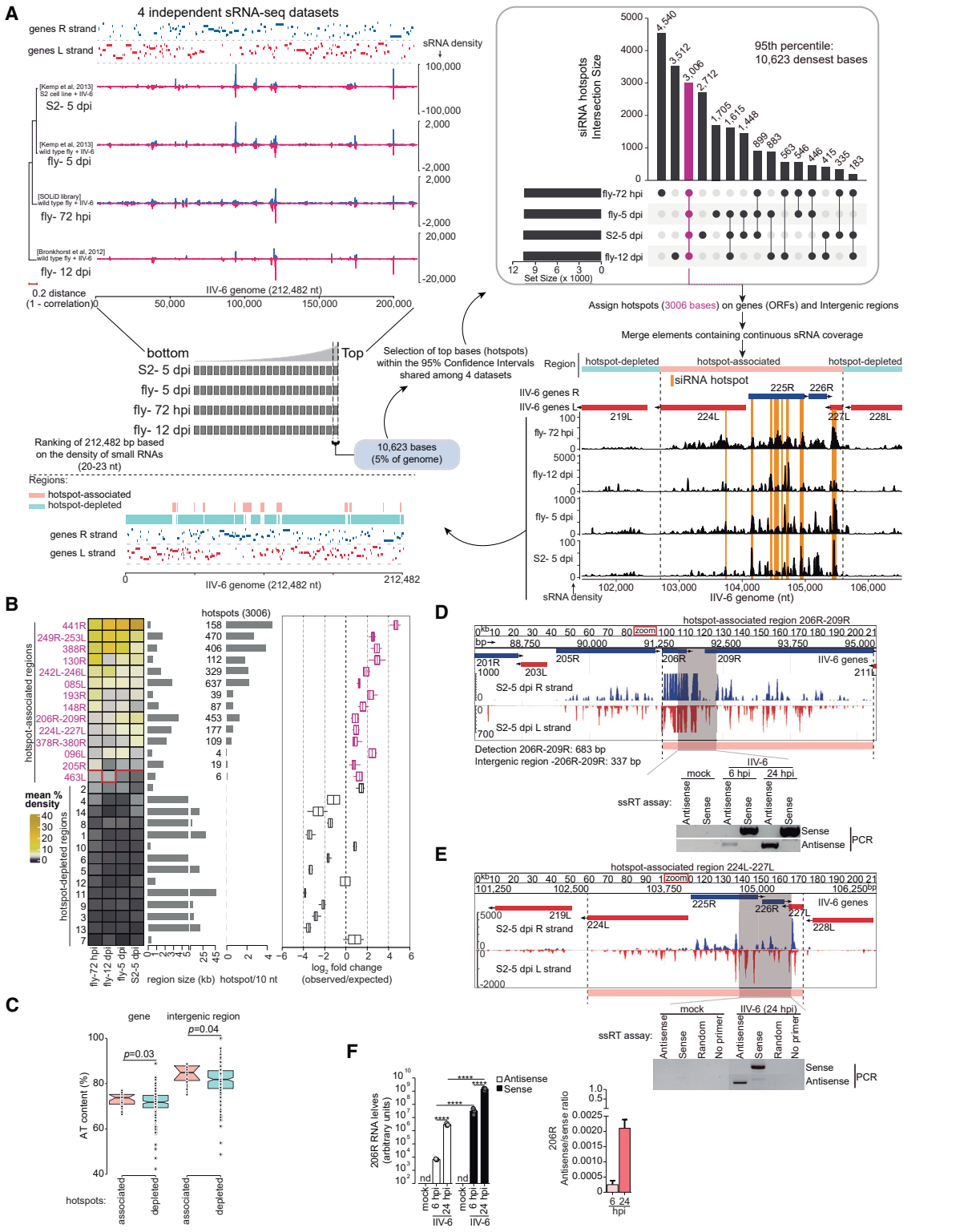

Figure 2. IIV-6-derived siRNAs are concentrated in a few genomic regions

(A) Computational strategy to identify regions on the IIV-6 genome associated with high density of siRNAs. The intersection of the top 5% most-covered bases in the viral genome shared among four independent small (s) RNA-seq datasets (3,006 bases) defined siRNA hotspots. These were used to define hotspot-associated regions with high sRNA coverage interspaced with hotspot-depleted regions. sRNAs (20–23 nt) mapping to the IIV-6 genome are represented as 8-bp bins.

(legend continued on next page)

AT-rich regions of the IIV-6 genome are more likely to generate dsRNA precursors that will be processed into siRNAs.

The size heterogeneity of hotspot-associated regions matches the diversity of dsRNA products observed in IIV-6-infected cells (Figure 1A). The largest hotspot-associated region with high siRNA density, 206R–209R, spanned 3,980 bp, including two genes (206R and 209R) and an intergenic region of 337 bp (Figure 2D). We observed continuous siRNA read coverage in the whole region, consistent with the idea that there is a single dsRNA precursor (Figure 2D). In this region, sense and antisense transcripts spanning the two ORFs and the intergenic region could be detected using strand-specific (ss) RT-PCR (Figure 2D). Another multigenic hotspot-associated region, 224L–227L, also generated long transcripts covering multiple ORFs and intergenic regions in both strands (Figure 2E). Notably, the 224L–227L region was quite distinct from 206R–209R in terms of ORF organization, since genes are encoded on both genomic strands, while 206R–209R is unidirectional. By quantitative ssRT-PCR (ssqRT-PCR), we observed that the sense strand was between 400 and 4,000 times more abundant than the antisense strand from 206R (gene within the 206R–209R region) at 6 and 24 hpi, respectively (Figure 2F). Likely, the sense strand detection was a sum of the regular viral transcript and the long RNA that spans the intergenic region. Antisense and sense transcripts from 206R were detected at 6 hpi, suggesting that dsRNAs can be produced early in the IIV-6 cycle even before they can be detected by immunoblot (Figures 2D and 2F).

Antisense transcription indicates genomic locations of dsRNA synthesis

Our results suggest that hotspot-associated regions in the IIV-6 genome produce sense and antisense transcripts that generate dsRNA. To test this idea, dsRNAs from mock- and IIV-6-infected cells were enriched by immunoprecipitation using an anti-dsRNA antibody (dsRIP) (Figures 3A and 3B). To validate the approach, we tested the protocol using cells infected with the RNA virus DCV and observed enrichment of dsRNA in the dsRIP (Figure S3A). Known sources of endogenous dsRNA such as TEs (DM297) and structured loci (AY119020 and CG18854) were also enriched in the dsRIP, suggesting the method could be used to characterize other dsRNAs (Figure 3C). To gain a genome-wide overview of viral dsRNA production, dsRIP samples from IIV-6-infected cells were subjected to high-throughput sequencing (dsRIP-seq) at 6 hpi. We also sequenced small RNAs from infected cells at the same time point for a direct comparison. We chose an early time point, 6 hpi, to try to analyze the biogenesis of dsRNA and siRNAs more directly and avoid secondary effects that accumulate over time. The profile of IIV-6-derived small RNAs at the early time point already showed a clear symmetrical size peak of 21 nt, characteristic of the siRNA response, and coverage along the IIV-6 genome correlated well with data from other time points (Figures S3B–S3D). We compared the abundance of antisense and sense transcripts from the dsRIP-seq data with the abundance of siRNAs from the sRNA-seq data (Figures 3D and 3E). There was positive correlation between siRNA and antisense transcript abundance (Figure 3E). Indeed, genomic coverage by siRNAs and antisense transcripts was qualitatively very similar (Figure 3F). The correlation between siRNA and antisense abundance was stronger for the hotspot-associated genomic regions (Figures 3D and 3E). These data show highly significant correlation between antisense coverage and siRNA biogenesis.

To further explore the relationship between antisense transcripts and siRNA biogenesis, we analyzed specific genomic regions. Hotspot-associated region 130R had the highest coverage of antisense transcripts and siRNAs at 6 hpi (Figure 3E). Unlike most of the other hotspot-associated regions, 130R is predicted to harbor a functional ORF in the antisense direction, suggesting that both strands are concomitantly transcribed, which would explain the high coverage by dsRNAs and siRNAs (Figure 3E, top). We also observed strong antisense transcript and siRNA coverage in the largest multigenic hotspot-associated regions, 206R–209R and 224L–227L (Figure 3G). Similar to endogenous dsRNAs, antisense RNAs from hotspot-associated regions were strongly enriched by dsRIP at 6 and 24 hpi, consistent with their origin from dsRNA (Figure 3H). As expected for dsRNA enrichment, the abundances of antisense and sense transcripts are more similar in the dsRIP compared with the input for 206R–209R and even for 130R, where bidirectional transcription leads to a more similar abundance of both strands (Figure S3E). In contrast, antisense transcripts derived from the 393L gene, located within hotspot-depleted region 13, were not enriched in the dsRIP, and the antisense-to-sense ratio did not change compared with input (Figures 3H and S3E). These results show that hotspot-associated regions correlate with sites of bidirectional transcription in the IIV-6 genome that can generate dsRNA.

IIV-6 genes from right (R) and left (L) genomic strands are shown on top. The datasets were clustered by a distance-like metric and represented as (1 − Pearson's correlation).

(B) Contribution of hotspot-associated or hotspot-depleted regions to the generation of IIV-6-derived siRNAs in four independent datasets. Hotspot-associated regions were numbered and named according to the presence of ORFs, while interspacing hotspot-depleted regions were numbered 1–14. Left: density map showing the density of siRNA coverage for each defined region (red line delimits 90% of the total density). Center: the number of hotspots in each region is depicted in the bar plot. Right: observed/expected siRNA abundance within hotspot-associated and hotspot-depleted regions. dpi, days post infection; hpi, hours post infection.

(C) Adenine-thymine (AT) content of genes and intergenic regions within hotspot-associated or hotspot-depleted regions. Unpaired t test was used to evaluate significance.

(D) JBrowse panel showing the siRNA density within hotspot-associated region 206R–209R. The segment highlighted between the 206R and the 209R genes, including a 337-bp intergenic region, was detected using strand-specific RT-PCR. sRNA coverages were clipped at 1,000 and 700 reads/base for R and L strands, respectively, to facilitate visualization.

(E) JBrowse panel showing the siRNA density within hotspot-associated region 224L–227L. The segment highlighted between the 225R and the 227L genes was detected using strand-specific RT-PCR.

(F) Antisense and sense quantification of 206R transcripts in IIV-6- or mock-infected S2 cells by ssqRT-PCR at indicated time points. Two-way ANOVA with Tukey's test (****$p < 0.0001$). The antisense/sense ratio is indicated on the right (n = 3 replicates/group).

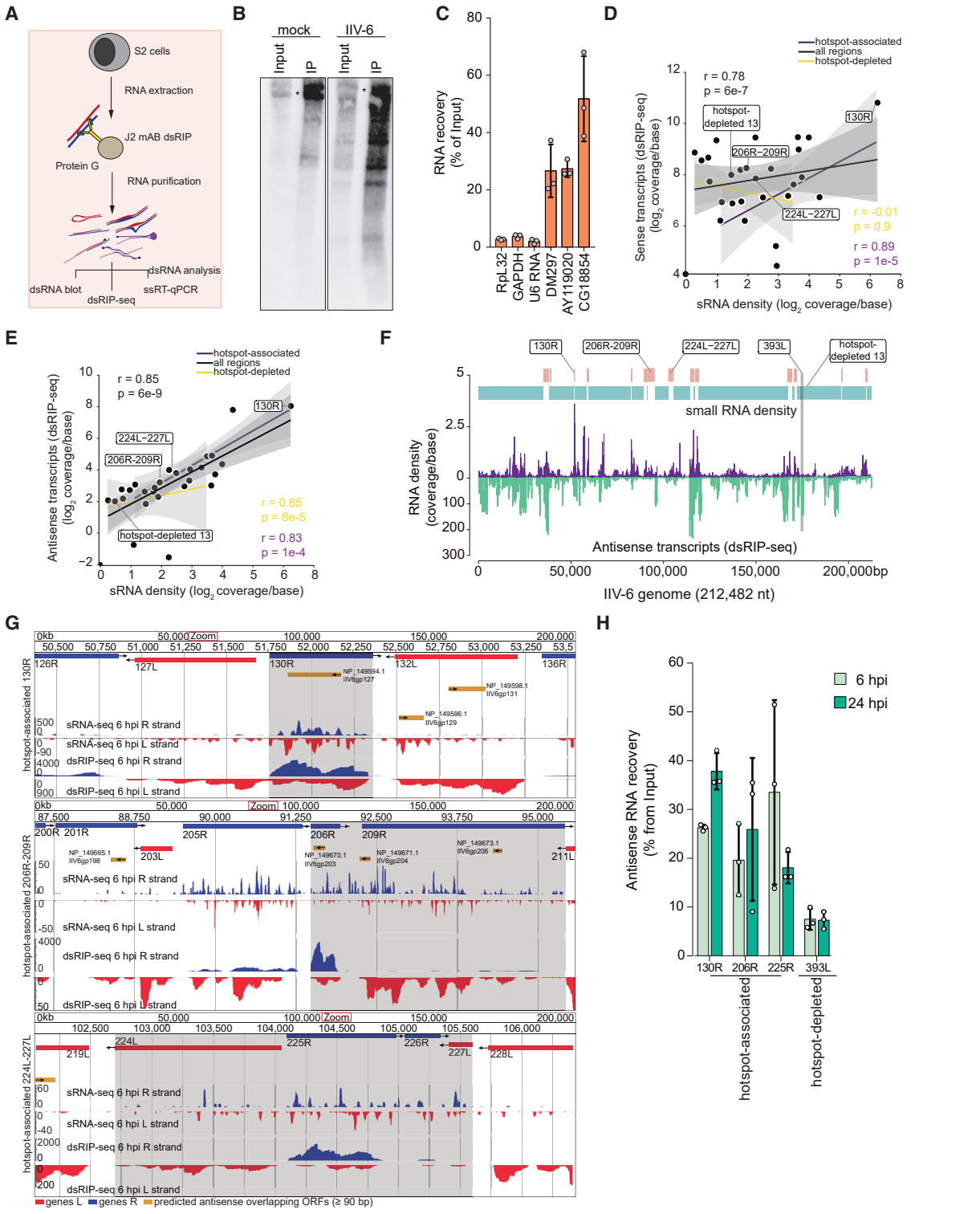

Figure 3. Correlation of dsRNA-generating regions and siRNA hotpots in the genome of IIV-6

(A) Strategy for dsRNA immunoprecipitation (dsRIP).

(B) dsRNA detection by immunoblotting after dsRIP of total RNA from mock- and IIV-6-infected cells. Total RNAs (10% input) are shown as a control. *Non-specific bands.

(C) Percentage of recovery of *Drosophila* genes (RpL32, GAPDH, U6 RNA) and endogenous dsRNAs (DM297, AY119020, CG18854) in the dsRIP (n = 3 replicates/group).

(legend continued on next page)

Invading DNA triggers dsRNA synthesis in the absence of viral proteins

Our results suggest that IIV-6-infected cells accumulate virus-derived dsRNAs. Thus, we tested whether IIV-6 generates dsRNA by a host mechanism in the absence of viral proteins (Figure 4A). To test this, we extracted genomic DNA (gDNA) from purified IIV-6 virion particles and transfected it into S2 cells. Iridovirus gDNA is not infectious, nor is it able to drive its replication (Willis et al., 1979). Accordingly, transfected gDNA levels declined after 24 h, in contrast to virion-infected cells, which experienced a large increase in DNA levels in the same period (Figure 4B). We determined if transfected gDNA generates viral transcripts from early and late stages of iridovirus replication (Figure 1C). As expected, gDNA transfection was not sufficient to induce significant levels of early (393L) and late (MCP; major capsid protein) viral genes, confirming that the IIV-6 genome requires viral proteins to initiate productive transcription and infection (Figure 4B). Interestingly, both 393L and MCP fall within hotspot-depleted regions (as indicated in Figure 4B). In contrast, transcripts derived from large multigenic hotspot-associated regions, 206R–209R and 224L–227L, were detected in the absence of viral replication at 6 and 24 h post gDNA transfection (Figures 4B and 4C). Notably, at 6 h, infected and transfected cells had similar levels of antisense transcripts from the 206R–209R region when viral gDNA levels were comparable (Figure 4C). At the same time, sense RNA levels were 4–5 orders of magnitude lower in transfected cells, suggesting that this is the contribution of viral transcription (Figures 4B and 4C). The data for other hotspot-associated regions, 224L–227L and 130R, also show the presence of sense and antisense transcripts in cells transfected with gDNA in the absence of viral replication (Figures S4A and S4B). In the case of 130R, RNA levels were ~1,000-fold higher during infection compared with transfection with gDNA, even at 6 hpi, suggesting a large contribution of active infection to the transcription of ORFs located in both strands (Figure S4B). Nevertheless, these data show that sense-antisense RNAs derived from hotspot-associated regions can originate from invading DNA in the absence of IIV-6 virion proteins.

Sense and antisense transcript levels increased over time during infection when the viral gDNA also increased (Figures 4C, S4A, and S4B). To study the contribution of viral replication to dsRNA synthesis, we evaluated the effects of inhibitors that directly or indirectly interfere with IIV-6 DNA replication (Figure S4C). S2 cells infected with IIV-6 virions were treated with AraC, a nucleoside analog that leads to premature termination of DNA synthesis, which blocked viral DNA replication (Figures 4D and S4C). We observed a mild effect on expression of early genes such as 393L, but a robust reduction in late gene transcription indicated by MCP levels (Figure S4E). AraC had a weaker effect on 206R–209R antisense transcript abundance compared with sense (Figures 4E and S4F). Similar results were observed for the 224L–227L region (Figure S4G). In the case of 130R, both sense and antisense transcripts were very sensitive to AraC, likely because the coding ORFs in both directions are late genes transcribed by the virus after DNA replication (Figure S4H). To confirm results using AraC, we also used phosphonoacetic acid (PAA), another inhibitor of DNA replication that had a similar effect on 206R–209R antisense transcript abundance compared with sense (Figures S4I–S4L). Together, these results suggest that viral DNA replication is not essential for antisense RNA production.

We observed that antisense RNAs can be made in the absence of virion proteins and viral DNA replication. However, synthesis of antisense RNAs could still require virus proteins made inside infected cells, such as the viral RNA polymerase (Figure 1C). To answer this question, we inhibited protein synthesis in infected cells by using cycloheximide (CHX). This treatment had only a modest effect on antisense transcript levels in contrast to its effects on sense transcripts from 206R–209R and 224L–227L, similar to the effect we observed with inhibitors of viral DNA replication (Figures 4F, S4G, and S4M). Again, 130R was more sensitive to CHX treatment, corroborating the idea that some of the bidirectional transcription of this region requires the viral polymerase (Figures S4H). However, more sensitive antisense RNAs from 130R had levels similar to those of 206R–209R and 224L–227L antisense RNAs under AraC and CHX treatments, indicating that this region can generate dsRNAs in the absence of viral proteins (Figures 4C, 4F, S4G, and S4H). As expected, CHX inhibited viral DNA replication and expression of the late genes but did not affect early transcription (Figures 4G and S4N). Thus, *de novo* viral protein synthesis is not essential for antisense transcription and, presumably, dsRNA accumulation.

Cellular RNA polymerase II generates IIV-6-derived dsRNAs

Our results suggest that IIV-6-derived antisense RNA is produced by a host RNA polymerase. Since the fly genome does not encode RNA-dependent RNA polymerases, dsRNA synthesis must be carried out by DNA-dependent RNA polymerases (RNAPs) (Figure 5A). We first assessed the general role of RNAPs in the synthesis of dsRNA precursors by using actinomycin D (ActD), a general inhibitor of RNAPs. ActD inhibited nuclear host RNAPs and had a direct effect on IIV-6 infection (Figures S5A and S5B). We also observed dose-response inhibition on the accumulation of sense and antisense transcripts from the 206R–209R and 130R regions, confirming that dsRNA precursors were generated *de novo* from iridovirus dsDNA by a

(D and E) Correlation of the abundance of IIV-6 sense (D) or antisense (E) transcripts in dsRIP-seq compared with siRNA density within hotspot-associated and hotspot-depleted regions at 6 hpi (n = 3 replicates pooled). Dots represent each region. Pearson's correlation for hotspot-associated and hotspot-depleted regions is indicated in purple and yellow, respectively, in addition to all regions combined in black.

(F) Coverage of small RNAs (20–23 nt) and antisense transcripts along the IIV-6 genome at 6 hpi in S2 cells (n = 3 replicates pooled).

(G) JBrowse panels showing density of coverage of sRNA-seq and dsRIP-seq for hotspot-associated regions 130R, 206R–209R, and 224L–227L at 6 hpi in S2 cells.

(H) Percentage of recovery of IIV-6 antisense transcripts from hotspot-associated regions 130R, 206R–209R (206R), and 224L–227L (225R) compared with hotspot-depleted region 13 (393L) in the dsRIP at indicated time points (n = 3 replicates/group).

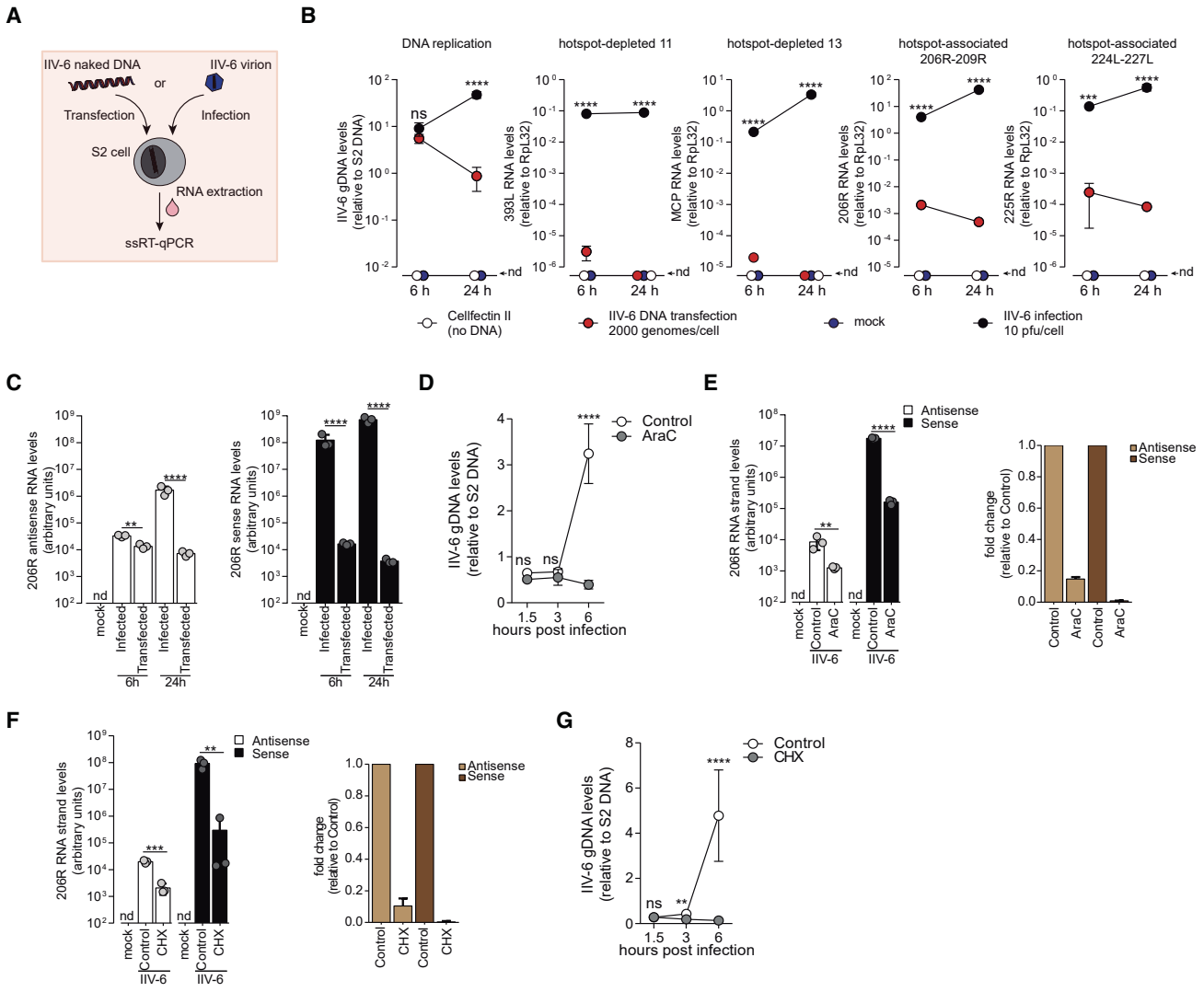

Figure 4. Recognition of naked DNA is sufficient to trigger host-dependent synthesis of dsRNAs

(A) Strategy to define the transcriptional origin of antisense/sense precursors of IIV-6-derived dsRNAs.

(B) Quantification of viral DNA replication and RNA transcription in cells infected with IIV-6 or transfected with viral genomic DNA (gDNA). Genes from hotspot-depleted (393L, MCP) and hotspot-associated regions 206R–209R (206R) and 224L–227L (225R) were analyzed by qRT-PCR (n = 3 replicates/time/group). nd, not detected. Two-way ANOVA with Sidak's test (ns, not significant; ***$p < 0.001$, ****$p < 0.0001$).

(C) Antisense and sense quantification of 206R transcripts by ssqRT-PCR at indicated time points in gDNA-transfected and IIV-6-infected S2 cells (n = 3 replicates/time/group). nd, not detected. Unpaired t test (**$p < 0.01$, ****$p < 0.0001$).

(D) Quantification of IIV-6 gDNA replication in control and cytosine β-D-arabinofuranoside-treated (AraC) S2 cells infected with IIV-6 at indicated time points (n = 3 replicates/time/group). Two-way ANOVA with Sidak's test (ns, not significant, ****$p < 0.0001$).

(E) Antisense and sense quantification of 206R transcripts by ssqRT-PCR in control and AraC-treated S2 cells infected with IIV-6 at 6 hpi (n = 3 replicates/group). nd, not detected. Unpaired t test (**$p < 0.01$, ****$p < 0.0001$).

(F) Antisense and sense quantification of 206R transcripts by ssqRT-PCR in control and cycloheximide-treated (CHX) S2 cells infected with IIV-6 at 6 hpi (n = 3 replicates/group). nd, not detected. Unpaired t test (**$p < 0.01$, ***$p < 0.001$).

(G) Quantification of IIV-6 gDNA replication in control and CHX-treated S2 cells infected with IIV-6 at indicated time points (n = 3 replicates/time/group). Two-way ANOVA with Sidak's test (ns, not significant; **$p < 0.01$, ****$p < 0.0001$).

host RNAP in infected cells (Figures 5B, S5C, and S5D). We next used α-amanitin (α-aman) and ML-60218, which are specific inhibitors of host RNAPII and RNAPIII, respectively. α-aman inhibited the accumulation of sense and antisense transcripts from the 206R–209R region, in a dose-dependent manner (Figure 5C). As a control, we observed that α-aman decreased levels of endogenous mRNAs such as GAPDH (Figure 5D). In contrast, ML-60218 led to no change in sense RNA levels and a slight increase in antisense RNAs (Figure 5E). As expected, ML-60218 led to a significant decrease in tRNA abundance (Figure 5F). We also observed a similar effect of α-aman on antisense transcripts from hotspot-associated regions 224L–227L and 130R

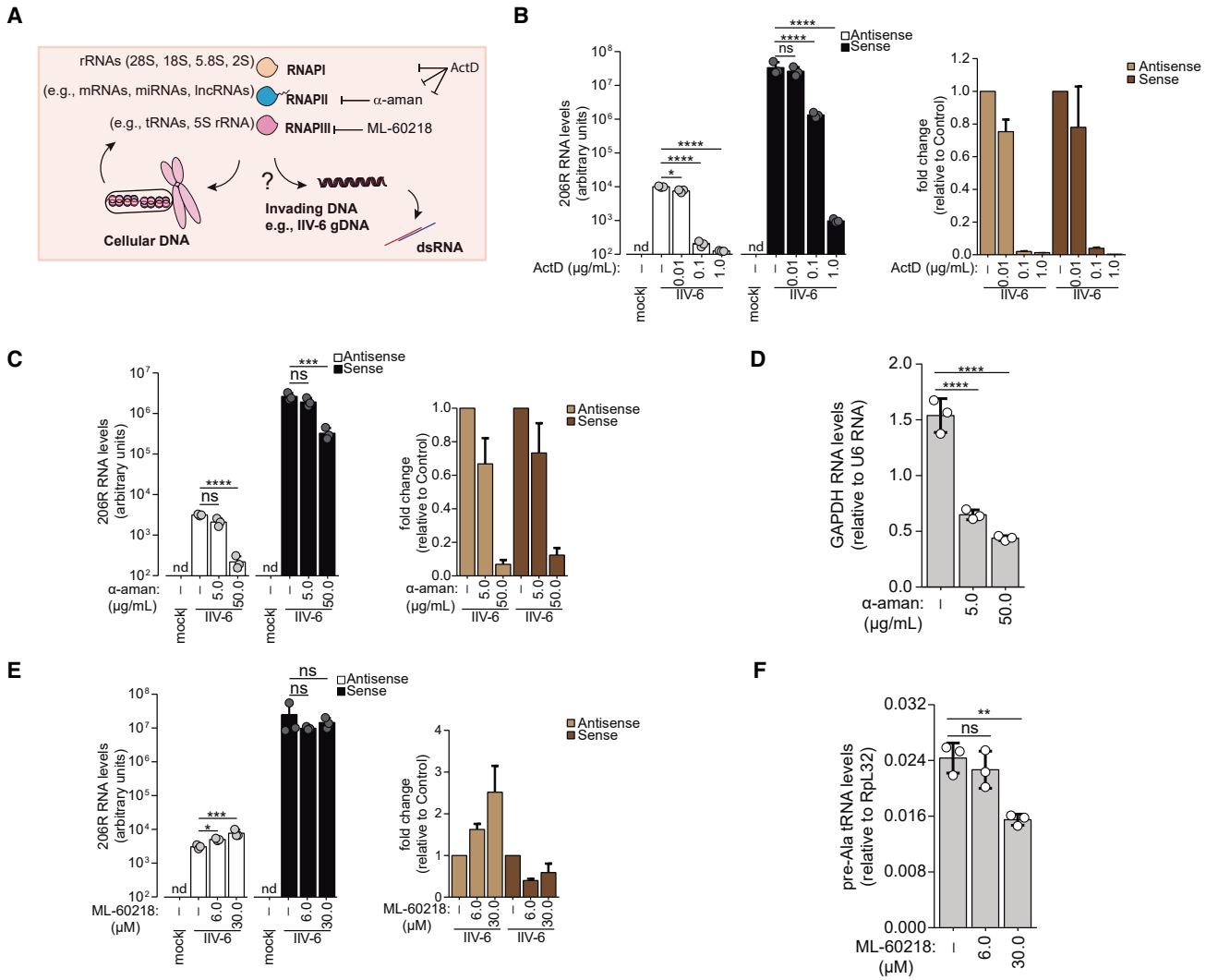

Figure 5. Host RNA polymerase II (RNAPII) synthesizes IIV-6-derived dsRNAs

(A) Overview of RNA species transcribed by the three animal RNA polymerases (RNAPI, RNAPII, and RNAPIII) and chemical inhibitors that target them.

(B) Antisense and sense quantification of 206R transcripts by ssqRT-PCR in control and actinomycin D-treated (ActD) S2 cells infected with IIV-6 at 6 hpi (n = 3 replicates/group). nd, not detected. One-way ANOVA with Dunnett's test (ns, not significant; *p < 0.05, ****p < 0.0001).

(C) Antisense and sense quantification of 206R transcripts by ssqRT-PCR in control and α-amanitin-treated (α-aman) S2 cells infected with IIV-6 at 6 hpi (n = 3 replicates/group). nd, not detected. One-way ANOVA with Dunnett's test (ns, not significant; ***p < 0.001, ****p < 0.0001).

(D) Levels of GAPDH RNA, an RNAPII transcript, in control and α-aman-treated S2 cells (n = 3 replicates/group). One-way ANOVA with Dunnett's test (****p < 0.0001).

(E) Antisense and sense quantification of 206R transcripts by ssqRT-PCR in control and RNAPIII inhibitor ML-60218-treated S2 cells infected with IIV-6 at 6 hpi (n = 3 replicates/group). nd, not detected. One-way ANOVA with Dunnett's test (ns, not significant; *p < 0.05, ***p < 0.001).

(F) Levels of pre-Ala-tRNA, an RNAPIII transcript, in control and ML-60218-treated S2 cells (n = 3 replicates/group). One-way ANOVA with Dunnett's test (ns, not significant; **p < 0.01).

(Figures S5E and S5F). α-aman also inhibited viral replication, while ML-60218 had no significant effects (Figures S5G and S5H). These results implicate RNAPII as the source of viral dsRNAs.

Virus-derived dsRNAs transcribed by host RNAPII activate antiviral RNAi

In *Drosophila*, the siRNA pathway can be triggered by endogenous and viral sources of dsRNAs. In the case of RNA viruses, these sources can be genetically discriminated by the requirement of the dsRBP Loqs-PD for the biogenesis of endogenous but not virus-derived siRNAs (Han et al., 2011a; Marques et al., 2010, 2013). Our results indicate that dsRNAs derived from IIV-6 are produced by the host RNAPII, which also produces precursors of endogenous siRNAs. Thus, we tested whether Loqs-PD would be required for recognition and processing of IIV-6-derived dsRNA. *loqs-PD*-deficient flies generated levels of IIV-6-derived siRNAs comparable to those of control flies

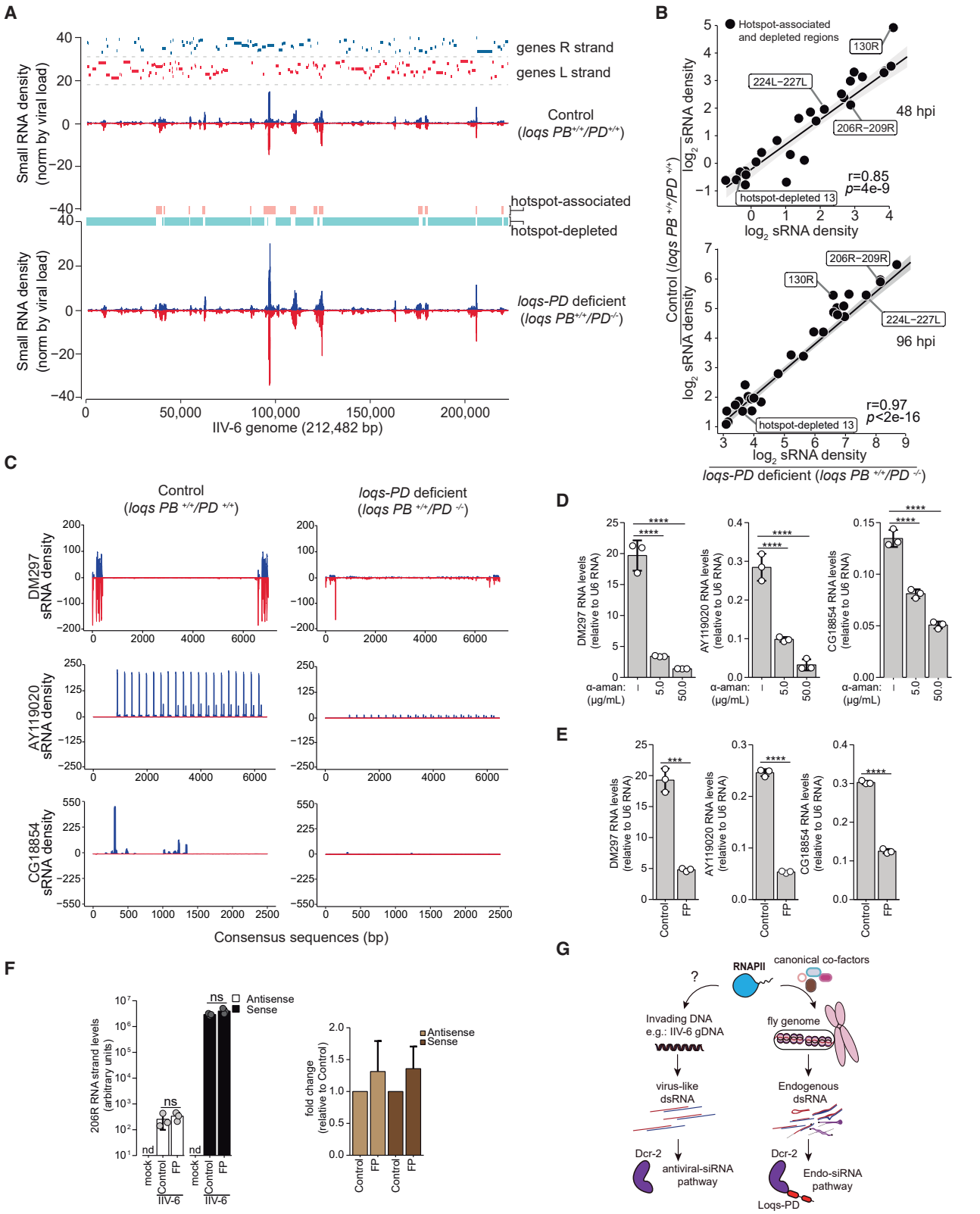

(legend on next page)

(Figures 6A, 6B, and S6A). Furthermore, we did not observe significant changes in siRNA abundance in any viral genomic region between Loqs-PD-deficient and control flies (Figure 6B). As described before, the same *loqs-PD*-deficient flies had a global decrease in the abundance of siRNAs derived from cis-NATs and Tes, while miRNAs remained comparable to wild type (Figures S6B–S6D) (Fukunaga et al., 2012). Endogenous siRNAs (endo-siRNAs) derived from structured loci AY119020 and CG18854, as well as TE DM297, showed a clear requirement for Loqs-PD, as previously reported in *Drosophila* (Figure 6C) (Fukunaga et al., 2012; Marques et al., 2010). These precursors of endo-siRNAs give rise to dsRNAs, as evident from their enrichment in the dsRIP (Figure 3C). Cells treated with α-aman had a significant decrease in RNA levels from these endogenous loci, confirming that they are RNAPII transcripts (Figure 6D). Even though endo-siRNA loci and IIV6-derived transcripts are both products of RNAPII, our results suggest that the siRNA pathway can discriminate dsRNAs derived from viral and host sources. Thus, we tested whether viral and host dsRNAs depend on similar RNAPII complexes by assessing the role of co-factors. Positive transcription elongation factor b (P-TEFb) is a complex containing cyclin-dependent kinase 9 (CDK9), which is an essential co-factor to control elongation of most RNAPII transcripts. P-TEFb can be inhibited by flavopiridol and the adenosine analog 5,6-dichloro-1-β-D-ribofuranosylbenzimidazole (DRB) (Chao et al., 2000; Chao and Price, 2001; Henriques et al., 2013; Marshall and Price, 1995). We observed that flavopiridol and DRB treatments efficiently reduced transcript levels of host endo-siRNA precursors at levels comparable to those of α-aman treatment (Figures 6E and S6E). In agreement with this observation, *cdk9* mutant larvae, lacking the catalytic subunit of P-TEFb, showed lower levels of endo-siRNAs derived from endogenous dsRNAs such as AY119020 and CG18854 (Figure S6F) (Church et al., 2017). In contrast, flavopiridol and DRB had limited or no effect on the levels of sense and antisense transcripts from viral hotspot-associated regions (Figures 6F and S6G). Flavopiridol (FP) and DRB had no effect on viral replication, but efficiently decreased the levels of host RNAPII transcripts (Figures S6H and S6I). These results connect P-TEFb-dependent RNAPII transcription of endo-siRNA precursors to Dcr-2 processing in a Loqs-PD-dependent manner. Notably, transcriptional elongation, which is regulated by P-TEFb, is also affected by the presence of the N6-methyladenosine (m^6A) modification in the nascent RNA (Henriques et al., 2013; Akhtar et al., 2021). Therefore, we analyzed the presence of the m^6A modification in endo-siRNA precursors such as cis-NATs and TEs. Based on genome-wide data of transcripts containing m^6A in *Drosophila*, we observed that cis-NATs were significantly enriched for the modification compared with other genes (Figure S6J) (Wang et al., 2021). In fact, over 95% of genes that generate cis-NATs had the m^6A modification. In regard to TEs, elements that contained the m^6A modification had a significantly higher odds ratio of generating siRNAs (Figure S6K). In addition, the abundance of siRNAs derived from TEs containing the m^6A modification was also significantly higher (Figure S6L). These results suggest that the presence of the m^6A modification in endogenous dsRNAs correlates with production of siRNAs. Together, these data suggest that transcription by the canonical P-TEFb RNAPII complex is associated with the presence of m^6A in the RNA, which directs processing by Dcr-2 in a Loqs-PD-dependent manner (Figure 6G). In contrast, a P-TEFb-independent RNAPII complex carries out transcription of viral dsRNA triggered by invading viral DNA to engage a Loqs-PD-independent siRNA pathway (Figure 6G).

DISCUSSION

Our work implicates the host RNAPII in the production of DNA virus-derived dsRNAs that function as signaling intermediates to activate antiviral RNAi in *Drosophila*. The RNAPII co-factor p-TEFb, which is required for the synthesis of most cellular transcripts, was dispensable for the production of virus-derived dsRNA (Henriques et al., 2013; Jonkers et al., 2014). This suggests that non-canonical RNAPII complexes generate dsRNAs that are intrinsically more likely to trigger antiviral RNA interference. Notably, transcription of precursors for dual *piwi*-interacting RNA (piRNA) clusters in the *Drosophila* germline is also mediated by RNAPII independent of several canonical transcription factors (Andersen et al., 2017; Chang et al., 2019). These non-canonical transcripts are preferred activators of the piRNA pathway in this case. The activation of RNAi pathways by RNAPII-derived products is conceptually similar to the role of mammalian RNAPIII in the production of 5′ triphosphate-containing dsRNAs using viral DNA as a template to trigger RIG-I sensing (Ablasser et al., 2009; Chiu et al., 2009). This suggests the independent convergence of host RNA polymerases in the recognition of invading viral DNA as a

Figure 6. Virus and endogenous dsRNAs are generated by distinct RNAPII complexes that trigger separate arms of the siRNA pathway

(A) Abundance of siRNAs from control (*loqs* $PB^{+/+}/PD^{+/+}$) and *loqs-PD*-deficient (*loqs* $PB^{+/+}/PD^{-/-}$) flies across the IIV-6 genome at 96 hpi (n = 3 flies pooled/group). Small RNAs (20–23 nt) mapping to the IIV-6 genome are represented as 8-bp bins. Hotspot-associated and hotspot-depleted regions are represented in light pink and light blue, respectively.

(B) Correlation of siRNA density in control and *loqs-PD*-deficient flies at 48 and 96 hpi (n = 3 flies pooled/group). Dots represent hotspot-associated and hotspot-depleted regions. Correlation was evaluated using Pearson's.

(C) Abundance of endogenous siRNAs (endo-siRNA) from DM297, a transposable element, and two structured loci, AY119020 and CG18854, in control and *loqs-PD*-deficient flies in samples described in (A).

(D) Quantification of DM297, AY119020, and CG18854 transcripts in control and α-aman-treated S2 cells by qRT-PCR (n = 3 replicates/group). One-way ANOVA with Dunnett's test (****$p < 0.0001$).

(E) Quantification of DM297, AY119020, and CG18854 transcripts in control and flavopiridol-treated (FP) S2 cells by qRT-PCR (n = 3 replicates/group). Unpaired t test (**$p < 0.001$, ****$p < 0.0001$).

(F) Antisense and sense quantification of 206R transcripts by ssqRT-PCR in control and FP-treated S2 cells infected with IIV-6 at 6 hpi (n = 3 replicates/group). nd, not detected. Unpaired t test (ns, not significant).

(G) Overview of activation of the siRNA pathway by IIV-6-derived and endogenous dsRNAs that are both products of host RNAPII.

strategy to engage antiviral dsRNA sensors. Here it is tempting to speculate that RNAPII products are longer and may be more adequate to activate Dcr-2 compared with shorter RNAPIII-synthesized RNAs that are triphosphorylated at the 5′, which are optimal RIG-I activators (Schlee et al., 2009).

Our findings are likely not restricted to IIV-6, since many insect DNA viruses generate siRNAs, including densoviruses, baculoviruses, nudiviruses, and poxviruses (Jayachandran et al., 2012; Ma et al., 2011; Sabin et al., 2013; Webster et al., 2015). These are very diverse DNA viruses with different genome structures, ranging from small single-stranded to large double-stranded circular and linear molecules. In addition, during infection by RNA viruses, the genome can be reverse transcribed into a viral DNA form capable of sustaining activation of the siRNA pathway (Goic et al., 2013; Poirier et al., 2018; Tassetto et al., 2017, 2019). In fact, triggering dsRNA synthesis may be a broader mechanism of DNA recognition in insects. Other DNA forms can generate dsRNA and induce an siRNA response in *Drosophila* cells, including the mitochondrial genome, plasmids, and even double-strand breaks in the nuclear genome (Merk et al., 2017; Michalik et al., 2012; Pajak et al., 2019). In these cases, the DNA is not coated with histones or other factors and therefore is more exposed, a feature that may facilitate recognition. Interestingly, DNA-virus-derived dsRNAs produced by RNAPII are recognized by Dcr-2 without the requirement for Loqs-PD. It is unclear whether Loqs-PD is involved in the recognition of dsRNA derived from other types of invading DNA, but the mechanism at work could be the same, since we showed that dsRNA synthesis does not require viral factors. In contrast to these invading DNAs, processing of endogenous sources of dsRNA by Dcr-2 requires Loqs-PD as a co-factor (Fukunaga et al., 2012; Marques et al., 2010). Our data indicate that endo-siRNA precursors are transcribed by a canonical p-TEFb-dependent RNAPII complex and are enriched for the m^6A modification. Since the presence of m^6A seems to prevent the formation of dsRNA, Loqs-PD may be required to stabilize endo-siRNA precursors and allow them to be processed by Dcr-2 (Gao et al., 2020; Kierzek et al., 2022; Qiu et al., 2021). It is also noteworthy that both P-TEFb (via CDK9) and m^6A are important for the recruitment of the microprocessor complex to long structured RNAs that are precursors of microRNAs, another class of endogenous small RNAs (Alarcón et al., 2015; Church et al., 2017). Similarly, P-TEFb and m^6A may be required to recruit Dcr-2 and Loqs-PD to endo-siRNA precursors. Thus, the biogenesis of endogenous small RNAs from endogenous dsRNAs may be tightly regulated by P-TEFb and m^6A to avoid potential toxicity.

IIV-6-derived dsRNAs seem to mostly accumulate in the nucleus of infected cells and outside of viral factories. This suggests that recognition of IIV-6 DNA by RNAPII occurs in the nucleus, unlike what has been suggested for RNAPIII in mammals (Ablasser et al., 2009; Chiu et al., 2009). It is also intriguing that recognition the IIV-6 gDNA triggers preferential transcription of specific regions of the genome by RNAPII. These regions are more AT rich than the rest of the genome, similar to the preference of RNAPIII for recognition of AT-rich DNA in mammalian cells (Ablasser et al., 2009; Chiu et al., 2009). In addition, we identified a specific AT-rich motif that is significantly enriched around hotspot-associated regions. This motif could be a signal for RNAPII recruitment and explain why these regions are preferentially targeted in the viral genome. Notably, the AT-rich motif we identified resembles conserved sequences that fold into hairpins at the 3′ ends of non-polyadenylated invertebrate iridovirus transcripts (İnce et al., 2017). Nevertheless, we have not observed a complete co-occurrence between the AT-rich motif and the presence of hairpins. Hence, dsRNA synthesis from invading DNA may be driven by accessibility to AT-rich sequences that are able to recruit RNAPII.

Overall, our work provides insight into the sensing of DNA viruses by the innate immune system through dsRNA recognition, a mechanism that likely preceded the evolution of DNA-sensing pathways.

Limitations of the study

Our results point to a role for a non-canonical RNAPII complex in the recognition of invading viral DNA that is used as a template for dsRNA synthesis to activate the siRNA pathway. Since activation of RNA interference is important to control IIV-6 infection, inhibition of RNAPII-dependent synthesis of viral dsRNA should have a proviral effect (Bronkhorst et al., 2019; Kemp et al., 2013). Unfortunately, we could not perform such experiments, since cell viability is affected by continuous RNAPII inhibition, which is required to measure production of new infectious particles. We are currently trying to identify specific components of the non-canonical RNAPII complex required for viral dsRNA synthesis that do not affect cellular transcription. This will allow us to directly assess the contribution of this non-canonical RNAPII complex to the control of IIV-6 infection. It will also be important to evaluate this mechanism in other insects, such as grasshoppers, that are naturally infected by IIV-6, as well as the importance of this mechanism in the antiviral defense against other DNA viruses (de Miranda et al., 2021).

STAR★METHODS

Detailed methods are provided in the online version of this paper and include the following:

- KEY RESOURCES TABLE
- RESOURCE AVAILABILITY
  - Lead contact
  - Materials availability
  - Data and code availability
- EXPERIMENTAL MODEL AND SUBJECT DETAILS
  - Fly stocks and infections
  - Viruses and cells
- METHOD DETAILS
  - Chemical inhibitors
  - DNA isolation from IIV-6 particles and DNA transfection
  - Immunofluorescence (IFA)
  - BrdU labeling of cellular DNA
  - *In vitro* synthesis of dsRNA
  - dsRNA immunoblotting
  - dsRNA enrichment by immunoprecipitation (dsRIP)
  - DNase I treatment of RNA samples
  - RNA analysis: cDNA synthesis, PCR and qPCR reactions

SUPPLEMENTAL INFORMATION

Supplemental information can be found online at https://doi.org/10.1016/j.celrep.2022.110976.

ACKNOWLEDGMENTS

We would like to thank all members of the Marques and Imler laboratories for invaluable assistance and discussions. We also thank Phillip D. Zamore for mutant flies, the Sequencing Platform of Strasbourg (University of Strasbourg) for high-throughput sequencing, and the UFMG microscopy facility (CAPI) for image acquisition. This work of the Interdisciplinary Thematic Institute IMCBio, as part of the ITI 2021-2028 program of the University of Strasbourg, CNRS, and Inserm, was supported by IdEx Unistra (ANR-10-IDEX-0002), by the SFRI-STRAT'US project (ANR 20-SFRI-0012), and by EUR IMCBio (IMCBio ANR-17-EURE-0023) under the framework of the French Investments for the Future Program as well as by the previous Labex NetRNA (ANR-10-LABX-0036). This work has also been supported by grants from the Conselho Nacional de Desenvolvimento Científico e Tecnológico, Fundação de Amparo à Pesquisa do Estado de Minas Gerais, Rede Mineira de Imunobiológicos (grant REDE-00140-16), Rede Mineira de Biomoléculas (grant REDE-00125-16), Instituto Nacional de Ciência e Tecnologia de Vacinas (INCTV), Institute for Advanced Studies of the University of Strasbourg (USIAS Fellowship 2019), and Fonds régionale de coopération pour la recherche FRCT2020 Région Grand-Est (ViroMod) to J.T.M. This study was financed in part by the Coordenação de Aperfeiçoamento de Pessoal de Nível Superior-Brasil (CAPES) - Finance Code 001 to J.T.M. I.S.J.F. was supported by fellowships from CNPq and CAPES. R.W.C. was supported by the NIH (R35GM118144).

AUTHOR CONTRIBUTIONS

J.T.M., J.-L.I., and R.W.C. conceived the study. I.J.S.F., R.P.O., and J.A.S. performed experiments. E.R.G.R.A. performed bioinformatic analysis with contributions from I.J.S.F. I.J.S.F. and J.A.S. performed and analyzed imaging experiments. L.D. contributed with IFA methods and analysis. J.-L.I. and J.T.M. supervised experiments and analysis. J.-L.I. and J.T.M. were responsible for funding acquisition. I.J.S.F., J.-L.I., and J.T.M. drafted the manuscript with contributions of all authors.

DECLARATION OF INTERESTS

The authors declare no competing interests.

Received: October 5, 2021
Revised: March 24, 2022
Accepted: May 26, 2022
Published: June 21, 2022

REFERENCES

Ablasser, A., Bauernfeind, F., Hartmann, G., Latz, E., Fitzgerald, K.A., and Hornung, V. (2009). RIG-I-dependent sensing of poly(dA:dT) through the induction of an RNA polymerase III-transcribed RNA intermediate. Nat. Immunol. *10*, 1065–1072. https://doi.org/10.1038/ni.1779.

Aguiar, E.R.G.R., Olmo, R.P., Paro, S., Ferreira, F.V., de Faria, I.J.D.S., Todjro, Y.M.H., Lobo, F.P., Kroon, E.G., Meignin, C., Gatherer, D., et al. (2015). Sequence-independent characterization of viruses based on the pattern of viral small RNAs produced by the host. Nucleic Acids Res. *43*, 6191–6206. https://doi.org/10.1093/nar/gkv587.

Akhtar, J., Renaud, Y., Albrecht, S., Ghavi-Helm, Y., Roignant, J.-Y., Silies, M., and Junion, G. (2021). m6A RNA methylation regulates promoter- proximal pausing of RNA polymerase II. Mol. Cell *81*, 3356–3367.e6. https://doi.org/10.1016/j.molcel.2021.06.023.

Alarcón, C., Goodarzi, H., Lee, H., Liu, X., Tavazoie, S., and Tavazoie, S.F. (2015). HNRNPA2B1 is a mediator of m(6)A-dependent nuclear RNA processing events. Cell *162*, 1299–1308. https://doi.org/10.1016/j.cell.2015.08.011.

Aloni, Y. (1972). Extensive symmetrical transcription of simian virus 40 DNA in virus-yielding cells. Proc. Natl. Acad. Sci. U S A *69*, 2404–2409. https://doi.org/10.1073/pnas.69.9.2404.

Andersen, P.R., Tirian, L., Vunjak, M., and Brennecke, J. (2017). A heterochromatin-dependent transcription machinery drives piRNA expression. Nature *549*, 54–59. https://doi.org/10.1038/nature23482.

Bailey, T.L., Johnson, J., Grant, C.E., and Noble, W.S. (2015). The MEME suite. Nucleic Acids Res. *43*, W39–W49. https://doi.org/10.1093/nar/gkv416.

Boone, R.F., Parr, R.P., and Moss, B. (1979). Intermolecular duplexes formed from polyadenylylated vaccinia virus RNA. J. Virol. *30*, 365–374. https://doi.org/10.1128/jvi.30.1.365-374.1979.

Bronkhorst, A.W., van Cleef, K.W.R., Vodovar, N., İnce, İ.A., Blanc, H., Vlak, J.M., Saleh, M.-C., and van Rij, R.P. (2012). The DNA virus Invertebrate iridescent virus 6 is a target of the Drosophila RNAi machinery. Proc. Natl. Acad. Sci. U S A *109*, E3604–E3613. https://doi.org/10.1073/pnas.1207213109.

Bronkhorst, A.W., Vogels, R., Overheul, G.J., Pennings, B., Gausson-Dorey, V., Miesen, P., and van Rij, R.P. (2019). A DNA virus-encoded immune antagonist fully masks the potent antiviral activity of RNAi in *Drosophila*. Proc. Natl. Acad. Sci. U S A *116*, 24296–24302. https://doi.org/10.1073/pnas.1909183116.

Buels, R., Yao, E., Diesh, C.M., Hayes, R.D., Munoz-Torres, M., Helt, G., Goodstein, D.M., Elsik, C.G., Lewis, S.E., Stein, L., and Holmes, I.H. (2016). JBrowse: a dynamic web platform for genome visualization and analysis. Genome Biol. *17*, 66. https://doi.org/10.1186/s13059-016-0924-1.

Burgess, H.M., and Mohr, I. (2015). Cellular 5'-3' mRNA exonuclease Xrn1 controls double-stranded RNA accumulation and anti-viral responses. Cell Host Microbe *17*, 332–344. https://doi.org/10.1016/j.chom.2015.02.003.

Chang, T.H., Mattei, E., Gainetdinov, I., Colpan, C., Weng, Z., and Zamore, P.D. (2019). Maelstrom represses canonical polymerase II transcription within Bi-directional piRNA clusters in Drosophila melanogaster. Mol. Cell *73*, 291–303.e6. https://doi.org/10.1016/j.molcel.2018.10.038.

Chao, S.-H., Fujinaga, K., Marion, J.E., Taube, R., Sausville, E.A., Senderowicz, A.M., Peterlin, B.M., and Price, D.H. (2000). Flavopiridol inhibits P-TEFb and blocks HIV-1 replication. J. Biol. Chem. *275*, 28345–28348. https://doi.org/10.1074/jbc.C000446200.

Chao, S.-H., and Price, D.H. (2001). Flavopiridol inactivates P-TEFb and blocks most RNA polymerase II transcription in vivo. J. Biol. Chem. *276*, 31793–31799. https://doi.org/10.1074/jbc.M102306200.

Chinchar, V.G., Yu, K.H., and Jancovich, J.K. (2011). The molecular biology of frog virus 3 and other iridoviruses infecting cold-blooded vertebrates. Viruses *3*, 1959–1985. https://doi.org/10.3390/v3101959.

Chiu, Y.-H., Macmillan, J.B., and Chen, Z.J. (2009). RNA polymerase III detects cytosolic DNA and induces type I interferons through the RIG-I pathway. Cell *138*, 576–591. https://doi.org/10.1016/j.cell.2009.06.015.

Chung, W.J., Okamura, K., Martin, R., and Lai, E.C. (2008). Endogenous RNA interference provides a somatic defense against Drosophila transposons. Curr. Biol. *18*, 795–802. https://doi.org/10.1016/j.cub.2008.05.006.

Church, V.A., Pressman, S., Isaji, M., Truscott, M., Cizmecioglu, N.T., Buratowski, S., Frolov, M.V., and Carthew, R.W. (2017). Microprocessor recruitment to elongating RNA polymerase II is required for differential expression of MicroRNAs. Cell Rep. *20*, 3123–3134. https://doi.org/10.1016/j.celrep.2017.09.010.

Czech, B., Malone, C.D., Zhou, R., Stark, A., Schlingeheyde, C., Dus, M., Perrimon, N., Kellis, M., Wohlschlegel, J.A., Sachidanandam, R., et al. (2008). An endogenous small interfering RNA pathway in Drosophila. Nature *453*, 798–802. https://doi.org/10.1038/nature07007.

de Faria, I.J.D.S., Olmo, R.P., Silva, E.G., and Marques, J.T. (2013). dsRNA sensing during viral infection: lessons from plants, worms, insects, and mammals. J. Interferon Cytokine Res. *33*, 239–253. https://doi.org/10.1089/jir.2013.0026.

de Miranda, J.R., Granberg, F., Low, M., Onorati, P., Semberg, E., Jansson, A., and Berggren, Å. (2021). Virus diversity and loads in crickets reared for feed: implications for husbandry. Front. Vet. Sci. *8*, 642085. https://doi.org/10.3389/fvets.2021.642085.

Deddouche, S., Matt, N., Budd, A., Mueller, S., Kemp, C., Galiana-Arnoux, D., Dostert, C., Antoniewski, C., Hoffmann, J.A., and Imler, J.-L. (2008). The DExD/H-box helicase Dicer-2 mediates the induction of antiviral activity in drosophila. Nat. Immunol. *9*, 1425–1432. https://doi.org/10.1038/ni.1664.

Dewitte-orr, S.J., and Mossman, K.L. (2010). dsRNA and the innate antiviral immune response. In Nathan and Oski's Hematology and Oncology of Infancy and Childhood, Eighth Edition, pp. 325–341. https://doi.org/10.2217/fvl.10.18.

Dhir, A., Dhir, S., Borowski, L.S., Jimenez, L., Teitell, M., Rötig, A., Crow, Y.J., Rice, G.I., Duffy, D., Tamby, C., et al. (2018). Mitochondrial double-stranded RNA triggers antiviral signalling in humans. Nature *560*, 238–242. https://doi.org/10.1038/s41586-018-0363-0.

Duesberg, P.H., and Colby, C. (1969). On the biosynthesis and structure of double-stranded RNA in vaccinia virus-infected cells. Proc. Natl. Acad. Sci. U S A *64*, 396–403. https://doi.org/10.1073/pnas.64.1.396.

Fukunaga, R., Han, B.W., Hung, J.-H., Xu, J., Weng, Z., and Zamore, P.D. (2012). Dicer partner proteins tune the length of mature miRNAs in flies and mammals. Cell *151*, 533–546. https://doi.org/10.1016/j.cell.2012.09.027.

Galiana-Arnoux, D., Dostert, C., Schneemann, A., Hoffmann, J.A., and Imler, J.-L. (2006). Essential function in vivo for Dicer-2 in host defense against RNA viruses in drosophila. Nat. Immunol. *7*, 590–597. https://doi.org/10.1038/ni1335.

Gao, Y., Vasic, R., Song, Y., Teng, R., Liu, C., Gbyli, R., Biancon, G., Nelakanti, R., Lobben, K., Kudo, E., et al. (2020). m6A modification prevents formation of endogenous double-stranded RNAs and deleterious innate immune responses during hematopoietic development. Immunity *52*, 1007–1021.e8. https://doi.org/10.1016/j.immuni.2020.05.003.

Ghildiyal, M., Seitz, H., Horwich, M.D., Li, C., Du, T., Lee, S., Xu, J., Kittler, E.L.W., Zapp, M.L., Weng, Z., and Zamore, P.D. (2008). Endogenous siRNAs derived from transposons and mRNAs in Drosophila somatic cells. Science *320*, 1077–1081. https://doi.org/10.1126/science.1157396.

Goic, B., Vodovar, N., Mondotte, J.A., Monot, C., Frangeul, L., Blanc, H., Gausson, V., Vera-Otarola, J., Cristofari, G., and Saleh, M.-C. (2013). RNA-mediated interference and reverse transcription control the persistence of RNA viruses in the insect model Drosophila. Nat. Immunol. *14*, 396–403. https://doi.org/10.1038/ni.2542.

Gordon, A., and Hannon, G.J. (2010). Fastx-toolkit. FASTQ/A short-reads preprocessing tools. (unpublished). http://hannonlab. cshl. edu/fastx_toolkit.

Hammond, S.M., Boettcher, S., Caudy, A.A., Kobayashi, R., and Hannon, G.J. (2001). Argonaute2, a link between genetic and biochemical analyses of RNAi. Science *293*, 1146–1150. https://doi.org/10.1126/science.1064023.

Han, Y.H., Luo, Y.J., Wu, Q., Jovel, J., Wang, X.H., Aliyari, R., Han, C., Li, W.X., and Ding, S.W. (2011a). RNA-based immunity terminates viral infection in adult Drosophila in the absence of viral suppression of RNA interference: characterization of viral small interfering RNA populations in wild-type and mutant flies. J. Virol. *85*, 13153–13163. https://doi.org/10.1128/JVI.05518-11.

Han, Y.-H., Luo, Y.-J., Wu, Q., Jovel, J., Wang, X.-H., Aliyari, R., Han, C., Li, W.-X., and Ding, S.-W. (2011b). RNA-based immunity terminates viral infection in adult Drosophila in the absence of viral suppression of RNA interference: characterization of viral small interfering RNA populations in wild-type and mutant flies. J. Virol. *85*, 13153–13163. https://doi.org/10.1128/JVI.05518-11.

Henriques, T., Gilchrist, D.A., Nechaev, S., Bern, M., Muse, G.W., Burkholder, A., Fargo, D.C., and Adelman, K. (2013). Stable pausing by RNA polymerase II provides an opportunity to target and integrate regulatory signals. Mol. Cell *52*, 517–528. https://doi.org/10.1016/j.molcel.2013.10.001.

Ilyin, Y.V., Chrneliauskaite, V., and Georgiev, G.P. (1980). Double-stranded sequences in RNA of Drosophila metanogaster: relation to mobile dispersed genes. Nucleic Acids Res. *8*, 3439–3457. https://doi.org/10.1093/nar/8.15.3439.

İnce, İ.A., Pijlman, G.P., Vlak, J.M., and van Oers, M.M. (2017). Hairpin structures with conserved sequence motifs determine the 3′ ends of non-polyadenylated invertebrate iridovirus transcripts. Virology *511*, 344–353. https://doi.org/10.1016/j.virol.2017.06.026.

Jacobs, B.L., and Langland, J.O. (1996). When two strands are better than one: the mediators and modulators of the cellular responses to double-stranded RNA. Virology *219*, 339–349. https://doi.org/10.1006/viro.1996.0259.

Jacquemont, B., and Roizman, B. (1975). RNA synthesis in cells infected with herpes simplex virus. X. Properties of viral symmetric transcripts and of double-stranded RNA prepared from them. J. Virol. *15*, 707–713. https://doi.org/10.1128/jvi.15.4.707-713.1975.

Jayachandran, B., Hussain, M., and Asgari, S. (2012). RNA interference as a cellular defense mechanism against the DNA virus baculovirus. J. Virol. *86*, 13729–13734. https://doi.org/10.1128/JVI.02041-12.

Jelinek, W., and Darnell, J.E. (1972). Double-stranded regions in heterogeneous nuclear RNA from hela cells. Proc. Natl. Acad. Sci. U S A *69*, 2537–2541. https://doi.org/10.1073/pnas.69.9.2537.

Jonkers, I., Kwak, H., and Lis, J.T. (2014). Genome-wide dynamics of Pol II elongation and its interplay with promoter proximal pausing, chromatin, and exons. Elife *3*, e02407. https://doi.org/10.7554/eLife.02407.

Kawamura, Y., Saito, K., Kin, T., Ono, Y., Asai, K., Sunohara, T., Okada, T.N., Siomi, M.C., and Siomi, H. (2008). Drosophila endogenous small RNAs bind to Argonaute 2 in somatic cells. Nature *453*, 793–797. https://doi.org/10.1038/nature06938.

Kemp, C., Mueller, S., Goto, A., Barbier, V., Paro, S., Bonnay, F., Dostert, C., Troxler, L., Hetru, C., Meignin, C., et al. (2013). Broad RNA interference-mediated antiviral immunity and virus-specific inducible responses in Drosophila. J. Immunol. *190*, 650–658. https://doi.org/10.4049/jimmunol.1102486.

Kierzek, E., Zhang, X., Watson, R.M., Kennedy, S.D., Szabat, M., Kierzek, R., and Mathews, D.H. (2022). Secondary structure prediction for RNA sequences including N6-methyladenosine. Nat. Commun. *13*, 1271. https://doi.org/10.1038/s41467-022-28817-4.

Kumar, M., and Carmichael, G.G. (1998). Antisense RNA: function and fate of duplex RNA in cells of higher eukaryotes. Microbiol. Mol. Biol. Rev. : MMBR *62*, 1415–1434. https://doi.org/10.1128/mmbr.62.4.1415-1434.1998.

Langmead, B., and Salzberg, S. (2012). Fast gapped-read alignment with Bowtie 2. Nat Methods *9*, 357–359. https://doi.org/10.1038/nmeth.1923.

Langmead, B., Trapnell, C., Pop, M., and Salzberg, S.L. (2009). Ultrafast and memory-efficient alignment of short DNA sequences to the human genome. Genome Biol. *10*, R25. https://doi.org/10.1186/gb-2009-10-3-r25.

Lee, Y.S., Nakahara, K., Pham, J.W., Kim, K., He, Z., Sontheimer, E.J., and Carthew, R.W. (2004). Distinct roles for Drosophila Dicer-1 and Dicer-2 in the siRNA/miRNA silencing pathways. Cell *117*, 69–81. https://doi.org/10.1016/s0092-8674(04)00261-2.

Liang, C., Wang, Y., Murota, Y., Smith, D., Siomi, M.C., Liu, Q., Liang, C., Wang, Y., Murota, Y., Liu, X., et al. (2015). TAF11 Assembles the RISC Loading Complex to Enhance RNAi Efficiency Article TAF11 Assembles the RISC

Loading Complex to Enhance RNAi Efficiency. Mol. Cell *59*, 1–12. https://doi.org/10.1016/j.molcel.2015.07.006.

Liu, Q., Rand, T.A., Kalidas, S., Du, F., Kim, H.-E., Smith, D.P., and Wang, X. (2003). R2D2, a bridge between the initiation and effector steps of the Drosophila RNAi pathway. Science *301*, 1921–1925. https://doi.org/10.1126/science.1088710.

Liu, S.-W., Katsafanas, G.C., Liu, R., Wyatt, L.S., and Moss, B. (2015). Poxvirus decapping enzymes enhance virulence by preventing the accumulation of dsRNA and the induction of innate antiviral responses. Cell Host Microbe *17*, 320–331. https://doi.org/10.1016/j.chom.2015.02.002.

Lucas, J.J., and Ginsberg, H.S. (1972). Identification of double-stranded virus-specific ribonucleic acid in KB cells infected with type 2 adenovirus. Biochem. Biophysical Res. Commun. *49*, 39–44. https://doi.org/10.1016/0006-291X(72)90006-X.

Ma, M., Huang, Y., Gong, Z., Zhuang, L., Li, C., Yang, H., Tong, Y., Liu, W., and Cao, W. (2011). Discovery of DNA viruses in wild-caught mosquitoes using small RNA high throughput sequencing. PLoS One *6*, e24758. https://doi.org/10.1371/journal.pone.0024758.

Marques, J.T., and Imler, J.L. (2016). The diversity of insect antiviral immunity: insights from viruses. Curr. Opin. Microbiol. *32*, 71–76. https://doi.org/10.1016/j.mib.2016.05.002.

Marques, J.T., Kim, K., Wu, P.-H., Alleyne, T.M., Jafari, N., and Carthew, R.W. (2010). Loqs and R2D2 act sequentially in the siRNA pathway in Drosophila. Nat. Struct. Mol. Biol. *17*, 24–30. https://doi.org/10.1038/nsmb.1735.

Marques, J.T., Wang, J.-P., Wang, X., de Oliveira, K.P.V., Gao, C., Aguiar, E.R.G.R., Jafari, N., and Carthew, R.W. (2013). Functional specialization of the small interfering RNA pathway in response to virus infection. PLoS Pathog. *9*, e1003579. https://doi.org/10.1371/journal.ppat.1003579.

Marshall, N.F., and Price, D.H. (1995). Purification of P-TEFb, a transcription factor required for the transition into productive elongation. J. Biol. Chem. *270*, 12335–12338. https://doi.org/10.1074/jbc.270.21.12335.

Martin, M. (2011). Cutadapt removes adapter sequences from high-throughput sequencing reads. EMBnet j *17*, 10. https://doi.org/10.14806/ej.17.1.200.

Merk, K., Breinig, M., Böttcher, R., Krebs, S., Blum, H., Boutros, M., and Förstemann, K. (2017). Splicing stimulates siRNA formation at Drosophila DNA double-strand breaks. PLoS Genet. *13*, e1006861. https://doi.org/10.1371/journal.pgen.1006861.

Michalik, K.M., Böttcher, R., and Förstemann, K. (2012). A small RNA response at DNA ends in Drosophila. Nucleic Acids Res. *40*, 9596–9603. https://doi.org/10.1093/nar/gks711.

Monsion, B., Incarbone, M., Hleibieh, K., Poignavent, V., Ghannam, A., Dunoyer, P., Daeffler, L., Tilsner, J., and Ritzenthaler, C. (2018). Efficient detection of long dsRNA in vitro and in vivo using the dsRNA binding domain from FHV B2 protein. Front. Plant Sci. *9*, 70. https://doi.org/10.3389/fpls.2018.00070.

Okamura, K., Chung, W.J., Ruby, J.G., Guo, H., Bartel, D.P., and Lai, E.C. (2008). The Drosophila hairpin RNA pathway generates endogenous short interfering RNAs. Nature *453*, 803–806. https://doi.org/10.1038/nature07015.

Pajak, A., Laine, I., Clemente, P., El-Fissi, N., Schober, F.A., Maffezzini, C., Calvo-Garrido, J., Wibom, R., Filograna, R., Dhir, A., et al. (2019). Defects of mitochondrial RNA turnover lead to the accumulation of double-stranded RNA in vivo. Plos Genet. *15*, e1008240. https://doi.org/10.1371/journal.pgen.1008240.

Peacock, N.J., Robinson, D.C., Forrest, M.J., Wilcock, P.D., and Sannikov, V.V. (1969). Measurement of the electron temperature by thomson scattering in tokamak T3. Nature *224*, 488–490. https://doi.org/10.1038/224488a0.

Perocchi, F., Xu, Z., Clauder-Münster, S., and Steinmetz, L.M. (2007). Antisense artifacts in transcriptome microarray experiments are resolved by actinomycin D. Nucleic Acids Res. *35*, e128. https://doi.org/10.1093/nar/gkm683.

Peyrefitte, C.N., Pastorino, B., Bessaud, M., Tolou, H.J., and Couissinier-Paris, P. (2003). Evidence for in vitro falsely-primed cDNAs that prevent specific detection of virus negative strand RNAs in dengue-infected cells: improvement by tagged RT-PCR. J. Virol. Methods *113*, 19–28. https://doi.org/10.1016/S0166-0934(03)00218-0.

Pfeffer, S., Zavolan, M., Grässer, F.A., Chien, M., Russo, J.J., Ju, J., John, B., Enright, A.J., Marks, D., Sander, C., and Tuschl, T. (2004). Identification of virus-encoded MicroRNAs. Science *304*, 734–736. https://doi.org/10.1126/science.1096781.

Plaskon, N.E., Adelman, Z.N., and Myles, K.M. (2009). Accurate strand-specific quantification of viral RNA. PLoS One *4*, e7468. https://doi.org/10.1371/journal.pone.0007468.

Poirier, E.Z., Goic, B., Tomé-Poderti, L., Frangeul, L., Boussier, J., Gausson, V., Blanc, H., Vallet, T., Loyd, H., Levi, L.I., et al. (2018). Dicer-2-Dependent generation of viral DNA from defective genomes of RNA viruses modulates antiviral immunity in insects. Cell Host Microbe *23*, 353–365.e8. https://doi.org/10.1016/j.chom.2018.02.001.

Qiu, W., Zhang, Q., Zhang, R., Lu, Y., Wang, X., Tian, H., Yang, Y., Gu, Z., Gao, Y., Yang, X., et al. (2021). N6-methyladenosine RNA modification suppresses antiviral innate sensing pathways via reshaping double-stranded RNA. Nat. Commun. *12*, 1582. https://doi.org/10.1038/s41467-021-21904-y.

Quinlan, A.R., and Hall, I.M. (2010). BEDTools: a flexible suite of utilities for comparing genomic features. Bioinformatics *26*, 841–842. https://doi.org/10.1093/bioinformatics/btq033.

Sabin, L.R., Zheng, Q., Thekkat, P., Yang, J., Hannon, G.J., Gregory, B.D., Tudor, M., and Cherry, S. (2013). Dicer-2 processes diverse viral RNA species. PLoS One *8*, e55458. https://doi.org/10.1371/journal.pone.0055458.

Schindelin, J., Arganda-Carreras, I., Frise, E., Kaynig, V., Longair, M., Pietzsch, T., Preibisch, S., Rueden, C., Saalfeld, S., Schmid, B., et al. (2012). Fiji: an open-source platform for biological-image analysis. Nat. Methods *9*, 676–682. https://doi.org/10.1038/nmeth.2019.

Schlee, M., Roth, A., Hornung, V., Hagmann, C.A., Wimmenauer, V., Barchet, W., Coch, C., Janke, M., Mihailovic, A., Wardle, G., et al. (2009). Recognition of 5' triphosphate by RIG-I helicase requires short blunt double-stranded RNA as contained in panhandle of negative-strand virus. Immunity *31*, 25–34. https://doi.org/10.1016/j.immuni.2009.05.008.

Schwarz, D.S., Du, T., Xu, Z., Aronin, N., and Zamore, P.D. (2003). Asymmetry in the assembly of the RNAi enzyme complex. Cell *115*, 199–208. https://doi.org/10.1016/S0092-8674(03)00759-1.

Son, K.-N., Liang, Z., and Lipton, H.L. (2015). Double-stranded RNA is detected by immunofluorescence analysis in RNA and DNA virus infections, including those by negative-stranded RNA viruses. J. Virol. *89*, 9383–9392. https://doi.org/10.1128/JVI.01299-15.

Tabeta, K., Georgel, P., Janssen, E., Du, X., Hoebe, K., Crozat, K., Mudd, S., Shamel, L., Sovath, S., Goode, J., et al. (2004). Toll-like receptors 9 and 3 as essential components of innate immune defense against mouse cytomegalovirus infection. Proc. Natl. Acad. Sci. U S A *101*, 3516–3521. https://doi.org/10.1073/pnas.0400525101.

Tassetto, M., Kunitomi, M., Tassetto, M., Kunitomi, M., and Andino, R. (2017). Circulating immune cells mediate a systemic RNAi-based adaptive antiviral response in Drosophila. Cell *169*, 314–325.e13. https://doi.org/10.1016/j.cell.2017.03.033.

Tassetto, M., Kunitomi, M., Whitfield, Z.J., Dolan, P.T., Sánchez-Vargas, I., Garcia-Knight, M., Ribiero, I., Chen, T., Olson, K.E., and Andino, R. (2019). Control of RNA viruses in mosquito cells through the acquisition of vDNA and endogenous viral elements. Elife *8*, e41244. https://doi.org/10.7554/eLife.41244.

Untergasser, A., Cutcutache, I., Koressaar, T., Ye, J., Faircloth, B.C., Remm, M., and Rozen, S.G. (2012). Primer3—new capabilities and interfaces. Nucleic Acids Res. *40*, e115. https://doi.org/10.1093/nar/gks596.

van Rij, R.P., Saleh, M.-C., Berry, B., Foo, C., Houk, A., Antoniewski, C., and Andino, R. (2006). The RNA silencing endonuclease Argonaute 2 mediates specific antiviral immunity in Drosophila melanogaster. Genes Dev. *20*, 2985–2995. https://doi.org/10.1101/gad.1482006.

Wang, X.-H., Aliyari, R., Li, W.-X., Li, H.-W., Kim, K., Carthew, R., Atkinson, P., and Ding, S.-W. (2006). RNA interference directs innate immunity against

viruses in adult Drosophila. Science *312*, 452–454. https://doi.org/10.1126/science.1125694.

Wang, Y., Zhang, L., Ren, H., Ma, L., Guo, J., Mao, D., Lu, Z., Lu, L., and Yan, D. (2021). Role of Hakai in m6A modification pathway in Drosophila. Nat. Commun. *12*, 2159. https://doi.org/10.1038/s41467-021-22424-5.

Weber, F., Wagner, V., Rasmussen, S.B., Hartmann, R., and Paludan, S.R. (2006). Double-stranded RNA is produced by positive-strand RNA viruses and DNA viruses but not in detectable amounts by negative-strand RNA viruses. J. Virol. *80*, 5059–5064. https://doi.org/10.1128/JVI.80.10.5059-5064.2006.

Webster, C.L., Waldron, F.M., Robertson, S., Crowson, D., Ferrari, G., Quintana, J.F., Brouqui, J.M., Bayne, E.H., Longdon, B., Buck, A.H., et al. (2015). The discovery, distribution, and evolution of viruses associated with Drosophila melanogaster. PLoS Biol. *13*, e1002210. https://doi.org/10.1371/journal.pbio.1002210.

Wickersheim, M.L., and Blumenstiel, J.P. (2013). Terminator oligo blocking efficiently eliminates rRNA from Drosophila small RNA sequencing libraries. BioTechniques *55*, 269–272. https://doi.org/10.2144/000114102.

Willis, D.B., Goorha, R., and Granoff, A. (1979). Nongenetic reactivation of frog virus 3 DNA. Virology *98*, 476–479. https://doi.org/10.1016/0042-6822(79)90572-5.

Zhang, J., Kobert, K., Flouri, T., and Stamatakis, A. (2014). PEAR: a fast and accurate Illumina Paired-End reAd mergeR. Bioinformatics *30*, 614–620. https://doi.org/10.1093/bioinformatics/btt593.

Zhang, S.-Y., Jouanguy, E., Ugolini, S., Smahi, A., Elain, G., Romero, P., Segal, D., Sancho-Shimizu, V., Lorenzo, L., Puel, A., et al. (2007). TLR3 deficiency in patients with herpes simplex encephalitis. Science *317*, 1522–1527. https://doi.org/10.1126/science.1139522.

Zhou, R., Czech, B., Brennecke, J., Sachidanandam, R., Wohlschlegel, J.A., Perrimon, N., and Hannon, G.J. (2009). Processing of Drosophila endo-siRNAs depends on a specific Loquacious isoform. RNA *15*, 1886–1895. https://doi.org/10.1261/rna.1611309.

STAR★METHODS

KEY RESOURCES TABLE

REAGENT or RESOURCE	SOURCE	IDENTIFIER
Antibodies		
Anti-dsRNA J2 monoclonal antibody (mAb)	English and Scientific Consulting Kft	Cat# 10010200; RRID: AB_2651015
Anti-dsRNA 9D5 rabbit IgG	Absolute antibody	Cat# Ab00458-23.0; RRID: AB_2920603
Anti-BrdU antibody	BD Biosciences	Cat# 555627; RRID: AB_395993
Anti-lamin Dm0	Developmental Studies Hybridoma Bank,	Cat# adl84.12 RRID: AB_528338
Donkey anti-mouse IgG (H+L) Highly CrossAdsorbed Secondary Antibody, Alexa Fluor Plus 488	Thermo Fisher Scientific	Cat#A32766; RRID: AB_2762823
Goat anti-Mouse IgG (H+L) Cross-Adsorbed Secondary Antibody, Alexa Fluor 488	Thermo Fisher Scientific	Cat#A-11001; RRID: AB_2534069
Goat anti-Rabbit IgG (H+L) Cross-Adsorbed Secondary Antibody, Alexa Fluor 546	Thermo Fisher Scientific	Cat# A-11010; RRID: AB_2534077
Anti-rabbit IgG, HRP-linked whole Ab (from donkey)	Amersham (GE Healthcare)	Cat# NA934; RRID: AB_772206
Bacterial and virus strains		
DCV	(Kemp et al., 2013)	N/A (not applicable)
IIV-6	(Kemp et al., 2013)	N/A
Chemicals, peptides, and recombinant proteins		
5,6-Dichlorobenzimidazole 1-β-D-ribofuranoside (DRB)	Sigma-Aldrich	Cat# D1916 CAS Number 53-85-0
α-amanitin (α-aman)	Sigma-Aldrich	Cat# A2263 CAS Number 23109-05-9
Actinomycin D (ActD)	Sigma-Aldrich	Cat# A1410 CAS Number: 50-76-0
Cycloheximide (CHX)	Sigma-Aldrich	Cat# C7698 CAS Number: 66-81-9
Cytosine β-D-arabinofuranoside (AraC)	Sigma-Aldrich	Cat# C1768 CAS Number: 147-94-4
Dimethyl sulfoxide (DMSO)	Sigma-Aldrich	Cat# D2650 CAS Number 67-68-5
Flavoperidol (FP)	Sigma-Aldrich	Cat# F3055 CAS Number 131740-09-5
ML-60218 (RNAPIII inhibitor)	Calbiochem	Cat# US1557403 CAS Number 577784-91-9
Phosphonoacetic acid (PAA)	Sigma-Aldrich	Cat# 284270 CAS Number 4408-78-0
TRIzol Reagent	Thermo Fisher Scientific	Cat# 15596018
Acid phenol-chloroform	Thermo Fisher Scientific	Cat# AM9720
Phenol:Chloroform:Isoamyl Alcohol (25:24:1, v/v)	Thermo Fisher Scientific	Cat# 15593031
RNaseOUT Recombinant Ribonuclease Inhibitor	Thermo Fisher Scientific	Cat# 10777019
Moloney murine leukaemia virus (M-MLV) Reverse Transcriptase	Promega	Cat# M1701
Hydromount medium	National Diagnostics	Cat# HS-106

(*Continued on next page*)

Continued

REAGENT or RESOURCE	SOURCE	IDENTIFIER
Hoechst *33342* DNA staining	Thermo Fisher Scientific	Cat# H-3570 CAS Number: 23491-52-3
Pierce 16% Formaldehyde (w/v), methanol-free	Thermo Fisher Scientific	Cat# 28906
SYBR Safe DNA Gel Stain	Thermo Fisher Scientific	Cat# S33102
Non-fat dry milk	Bio-Rad	Cat# 1706404
dNTP Set (100 mM each A,C,G,T)	GE Healthcare	Cat# 28406552
3 M Sodium Acetate solution	Thermo Fisher Scientific	Cat# AM9740
Critical commercial assays		
SUPERSCRIPT III	Thermo Fisher Scientific	Cat# 18080044
Power SYBR™ Green PCR Master Mix	Thermo Fisher Scientific	Cat# 4367659
TruSeq Small RNA Library Preparation Kit	Illumina	Cat# RS-200-0012
SOLiD total RNA expression kit	Thermo Fisher Scientific	Cat# 4445374
TruSeq Stranded Total RNA Library Prep Kit with Ribo-Zero Gold	Illumina	Cat# RS-122-2301
RNA 6000 Nano Kit	Agilent Technologies	Cat# 5067-1511
DNase I (RNase-free)	Thermo Fisher Scientific	Cat# AM2222
Exonuclease I	Thermo Fisher Scientific	Cat# EN0581
RNaseOUT Recombinant Ribonuclease Inhibitor	Thermo Fisher Scientific	Cat# 10777019
Moloney murine leukemia virus (M-MLV) Reverse Transcriptase	Promega	Cat# M1701
Phusion DNA polymerase	Thermo Fisher Scientific	Cat# F530S
Platinum Pfx DNA polymerase	Thermo Fisher Scientific	Cat# 11708021
MEGAscript™ T7 Transcription Kit	Thermo Fisher Scientific	Cat# AM1334
Dynabeads Protein G	Thermo Fisher Scientific	Cat# 10003D
Cellfectin II Reagent	Thermo Fisher Scientific	Cat# 10362100
Penicillin-Streptomycin (100X)	Thermo Fisher Scientific	Cat# 15070063
GlutaMAX	Thermo Fisher Scientific	Cat# 35050061
Schneider's *Drosophila* Medium	Thermo Fisher Scientific	Cat# 21720024
Fetal Serum bovine	Thermo Fisher Scientific	Cat# 12657029
Fetal Serum bovine	GE healthcare	Cat# SV30160
Deposited data		
The raw small RNQ-seq and dsRIP-seq data	This manuscript	SRA accession number: RJNA768250
Experimental models: Cell lines		
Drosophila Kc167 cells	Laboratory of Jean-Luc Imler (Université de Strasbourg)	FlyBase ID: FBtc0000001
Drosophila S2*	Laboratory of Richard W. Carthew (Northwestern University)	FlyBase ID: FBtc9000011
Experimental models: Organisms/strains		
D. melanogaster Strain w^{1118}	https://bdsc.indiana.edu/	RRID: BDSC_3605, 5905, 6326
w[1118];loqs[KO]/CyO;P{w+, FLAG-loqs-PB}/TM3, Sb[1]	(Fukunaga et al., 2012)	N/A
w[1118];loqs[KO]/CyO;P{w+, FLAG-loqs-PB-PD}/TM3, Sb[1]	(Fukunaga et al., 2012)	N/A
Oligonucleotides		
2 S rRNA Block DNA Oligo: 5′-TAC AAC CCT CAA CCA TAT GTA GTC CAA GCA/3SpC3/-3′	(Wickersheim and Blumenstiel, 2013)	N/A
Oligos for ssRT, PCR, dsRNA synthesis and qPCR assays	This manuscript	Table S1

(*Continued on next page*)

Continued

REAGENT or RESOURCE	SOURCE	IDENTIFIER
Random primers	Thermo Fisher Scientific	Cat# 48190-011
Software and algorithms		
Fiji (ImageJ)	(Schindelin et al., 2012)	fiji.sc/
Illustrator	Adobe	www.adobe.com/
Photoshop	Adobe	www.adobe.com/
Graphpad	GraphPad Software Inc.	https://www.graphpad.com/
Primer3plus	(Untergasser et al., 2012)	primer3plus.com/
JBrowse	(Buels et al., 2016)	jbrowse.org/
Bowtie2	(Langmead and Salzberg, 2012)	http://bowtie-bio.sourceforge.net/bowtie2/index.shtml
Bowtie	(Langmead et al., 2009)	http://bowtie-bio.sourceforge.net/index.shtml
Cutadapt v1.12	(Martin, 2011)	https://cutadapt.readthedocs.io/en/v1.12/
FASTX-Toolkit	http://hannonlab.cshl.edu/fastx_toolkit/	N/A
PEAR	(Zhang et al., 2014)	https://cme.h-its.org/exelixis/web/software/pear/
BEDTools	(Quinlan and Hall, 2010)	https://bedtools.readthedocs.io/en/latest/
Zen 3.1 Lite software	Carl Zeiss, Inc.	https://www.zeiss.com/microscopy/int/products/microscope-software/zen-lite.html
R software	The R Foundation	https://www.r-project.org/
Other		
Original codes	Eric R. G. R. Aguiar	https://github.com/ericgdp/dmel_and_IIV6
Images of immunofluorescence, gels, and blots	This manuscript	Under request
sRNA-seq from flies and S2 cells infected with IIV-6 (public data)	Bronkhorst et al., 2012; Kemp et al., 2013	Table S2
sRNA-seq from *cdk9* mutant larvae (public data)	Church et al., 2017	Table S2

RESOURCE AVAILABILITY

Lead contact

Further information and requests for resources and reagents should be directed to and will be fulfilled by the Lead Contact, João Trindade Marques (jtm@ufmg.br).

Materials availability

This study did not generate new unique reagents.

Data and code availability

The raw small RNA-seq and dsRIP-seq data with annotation and identification files have been deposited in SRA: PRJNA768250. Original codes have been deposited at GitHub: https://github.com/ericgdp/dmel_and_IIV6, and is publicly available as of the date of publication. Any additional information required to analyze the data reported in this paper is available from the lead contact upon request.

EXPERIMENTAL MODEL AND SUBJECT DETAILS

Fly stocks and infections

Fly stocks were grown on standard cornmeal-agar molasses at 25°C. *Loquacious* transgenic flies were described elsewhere (Fukunaga et al., 2012). Two transgenic lines expressing loqs specific isoforms were used here: *loqs-PD* deficient (w[1118]; loqs[KO]/CyO;

P{w+,FLAG-loqs-PB}/TM3,Sb[1]) and the Control (w[1118]; loqs[KO]/CyO; P{w+,FLAG-loqs-PB-PD}/TM3,Sb[1]) (Fukunaga et al., 2012). For IIV-6 infections, 4 to 6-day-old female flies were intrathoracic injected (Nanoject II injector; Drummond Scientific) with 5 X 10^5 $TCID_{50}$ (w[1118] flies for SOLiD platform sequencing) or 5,000 $TCID_{50}$ (Control and *loqs-PD* deficient flies for Illumina platform sequencing) diluted in 69 nL of non-supplemented Schneider's medium. The flies were incubated at 25°C and harvested in TRIzol reagent (Invitrogen). Samples were homogenized using a mini-Beadbeater homogenizer (BioSpec). RNA and DNA were extracted according to TRIzol's protocol.

Viruses and cells

Drosophila S2 cells were grown in Schneider's *Drosophila* medium supplemented with 10% heat-inactivated Fetal Bovine Serum (FBS, Gibco), 1X GlutaMAX (Gibco), and 1X penicillin/streptomycin (10 mg.mL^{-1}/10,000 U, Gibco). Cells were incubated at 25–28°C for regular growth and viral infections.

IIV-6 stock was produced in S2 cells using a multiplicity of infection of 0.001 pfu/cell with incubation for 5–6 days for virus growth. Cells were disrupted by freezing/thawing and IIV-6 was concentrated in 30% (wt/vol) sucrose cushion by ultracentrifugation. The blue opalescent IIV-6 pellet was resuspended in 1 X phosphate-buffered saline (1X PBS) (137 mM NaCl, 2.7 mM KCl, 10 mM Na_2HPO_4, 1.8 mM KH_2PO_4 [pH 7.4]) (Sigma) and spun down to remove particle aggregates. IIV-6 titer was determined in S2 cells incubated at 25°C for 8–10 days. IIV-6 Cytopathic Effect (CPE) was daily scored based on the decreasing of cell proliferation, the presence of large cells and/or cell debris. The Reed–Muench method was applied to calculate the 50% tissue culture–infective dose ($TCID_{50}$/mL) and converted to pfu/mL with a conversion factor of 0.7.

DCV stock was prepared from low-passage growth in S2 cells, purified by ultracentrifugation and resuspended in 10 mM Tris buffer, pH 7.5. The DCV titers were determined by end-point dilution using *Drosophila* Kc167 cells as previous described (Kemp et al., 2013). The CPE of DCV-infected cells was monitored and the titers calculated as pfu/mL.

For infections, S2 cells were counted, transferred to conical tubes, and infected with IIV-6, DCV or mock-infected according to each experimental setup. After infection, S2-infected cells were incubated at 25–28°C with periodic homogenization (10–10 min) to allow virus adsorption. Cells were then gently spun down at 200 g/4°C/5 min and the medium removed. Cells were resuspended in fresh Schneider's medium and seeded into 6 or 24-well plates. Infected cells were incubated at 25–28°C and harvested according to each experiment setup. Cell pellets were homogenized in TRIzol (Invitrogen) and RNA and DNA extracted according to the manufacturer's instructions. DCV infections were essentially carried as IIV-6 infections using 1 or 0.1 pfu/cell and harvested at 24 and 48 hpi, respectively.

METHOD DETAILS

Chemical inhibitors

CHX, ActD, DRB, flavopiridol and ML-60218 stocks were prepared in DMSO; BrdU, α-aman, AraC and PAA stocks were prepared in sterile water. For S2 treatment, ActD (0.01, 0.1 or 1 μg/mL), CHX (10 μg/mL), PAA (100 μg/mL) and AraC (200 μg/mL) were added concomitantly with IIV-6 infection. DBR (100 μM) and flavopiridol (0.5 μM) were added 15 min and 2 h before IIV-6 infection, respectively. α-amanitin (5 or 50 μg/mL) and ML-60218 (6 or 30 μM) were added 4 h before infection. In all cases cells were infected using 10 pfu/cell. After 1 h to allow IIV-6 adsorption, cells were spun down at 200 g/4°C/5 min and fresh Schneider's medium containing the same drugs was renewed. DMSO or water were used in control samples and adjusted to the highest dose of the drug. 20 μM BrdU were added concomitantly with IIV-6 when cells were processed 6 hpi for Immunofluorescence (IFA) or, in the case of 72 hpi, cells were infected with 0.01 pfu/cell and BrdU was added 2 h prior to cell fixation. To analyze endogenous transcripts, α-amanitin and ML-60218 were added 10 h before collecting the cells.

DNA isolation from IIV-6 particles and DNA transfection

IIV-6 was extracted from purified particles using Phenol:Chloroform:Isoamyl Alcohol (25:24:1 v/v, Invitrogen) and quantified using a Multiskan Microplate Spectrophotometer (Thermo). For DNA transfection, 8 μL of Cellfectin II Reagent (Invitrogen) were mixed to 100μL of non-supplemented Schneider medium. Cellfectin solution was mixed with 1 μg of purified IIV-6 DNA (~2000 genomes) or sterile water (mock) in 125 μL of non-supplemented Schneider medium and incubated for 15 min at Room Temperature (RT). S2 cells were counted, spun down, resuspended in fresh Schneider's medium supplemented with 1.5% of FBS in the absence of antibiotics (plating medium). Then, 2 × 10^6 cells were transferred into 6-well plates. The transfection solution was added into S2 cells with incubation for 3 h and plating medium replaced for complete Schneider medium (10% FBS, 1X Glutamax and 1X antibiotics). In parallel, S2 cells were infected with IIV-6 using 10 pfu/cell, as described above. Cells were harvested at 6 and 24 h post transfection/infection for RNA and DNA extraction using TRIzol.

Immunofluorescence (IFA)

Drosophila S2 cells were infected with 0.01 pfu/cell of IIV-6 for dsRNA staining and BrdU labelling (72 hpi) or 10 pfu/cell for BrdU labelling (6 hpi). 1 h before fixation, S2 cells were homogenized and transferred to coverslips treated with Concanavalin A or Poly-L-lysine (Sigma) and incubated for 30–60 min to allow cell attachment. Cells were fixed with 4% formaldehyde (Pierce), washed in 1X PBS and permeabilized twice with 0.1% Triton X-100 in 1X PBS (PBSTX) for 10 min. Cells were blocked with 10% of FBS in

PBSTX (blocking buffer) for 1 h at RT. Primary antibodies were diluted in blocking buffer and incubated with cells at 4°C/overnight. The antibodies anti-dsRNA 9D5 (Absolute antibody), anti-*Drosophila* Lamin Dm0 (Developmental Studies Hybridoma Bank) and anti-BrdU antibody (BD, clone 3D4) were 2000, 200 and 400-fold diluted, respectively. Cells were washed three times with PBSTX. Secondary Goat IgG (H+L) conjugated with Alexa Fluor 488 (anti-mouse), Donkey IgG (H+L) Alexa Fluor Plus 488 (anti-mouse) and/or Goat IgG (H+L) conjugated with Alexa Fluor 546 (anti-rabbit) antibodies at 400-fold dilution in PBSTX were associated to Hoechst 33342 DNA staining (Molecular Probes) and incubated with cells for 1 h at RT. When present, 100-fold diluted Phalloidin conjugated with Alexa Fluor 488 (Molecular Probes) was added in secondary antibody solution. Cells were washed three times with PBSTX and rinsed once with 1X PBS. Coverslips were mounted in microscope slides with Hydromount medium (National Diagnostics) and sealed with nail polish. Imaging was performed using adapted settings on a Zeiss LSM880 confocal microscope. Images were processed in ImageJ and the final panel mounted in PhotoShop (Schindelin et al., 2012).

BrdU labeling of cellular DNA

To label replicative S2 DNA with BrdU, an additional DNA hydrolysis step was performed in the immunofluorescence to allow the anti-BrdU antibody access the protected cellular dsDNA. Fixed S2 cells were treated with 0.5 M HCl for 30 min at RT, the HCl was then removed and neutralized with 0.1 M sodium borate buffer pH 8.5 for 30 min. The sodium borate buffer was removed from slides and cells washed with 1X PBS. Subsequent steps were performed as described above for IFA in S2 cells.

In vitro synthesis of dsRNA

PCR products for *in vitro* synthesis of dsGFP were generated from plasmid templates using primers containing the T7 polymerase recognition sequence in their 5′-ends. PCR products were purified using Phenol:Chloroform:Isoamyl Alcohol (25:24:1 v/v). dsRNAs were synthesized from purified PCR products using MegaScript T7 transcription kit (Invitrogen), purified using Acid Phenol (Invitrogen) and annealed (20 mM Tris-HCl pH7.5, 100 mM NaCl). Size and annealing efficiency were evaluated in 2% agarose gel stained with Ethidium Bromide.

dsRNA immunoblotting

Total RNA was quantified using Nanodrop (Thermo), mixed to 6X DNA loading buffer (Invitrogen) and then resolved on 3.5% non-denaturing polyacrylamide gels. Samples were wet transferred to a positively charged nylon membrane (GE) in TBE 0.5X at 35 V/4°C/overnight. The RNAs were crosslinked to the membrane using 120 mJ/cm^2 UVC (Stratagene). Membranes were washed in 1X PBS and incubated in the blocking buffer consisted of PBST (1X PBS and 0.1% Tween-20), 5% of non-fat skim milk (Bio-Rad), 50 μg/mL sheared salmon DNA. After 1 h shaking at RT, blocking buffer was replaced for the primary antibody solution consisting of PBST, 2% non-fat skim milk and 1/6000 of recombinant rabbit anti-dsRNA 9D5 antibody (Absolute antibody). Membranes were incubated for 2 h shaking at RT, washed with PBST and incubated for 1 h shaking at RT in the 1/10000 of HPR-linked anti-rabbit antibody (Amersham) solution (1X PBST, 2% non-fat skim milk). The membranes were washed with PBST and rinsed in 1X PBS. Then, the ECL substrate (GE) was added to blots according to the manufacturer's recommendations. Chemiluminescent signals were acquired using a Fusion FX7 Image System. Data were analyzed with ImageJ software. dsRNA sizes were estimated based on the pattern of purified dsRNAs from DCV-infected cells in an 1% agarose gel.

dsRNA enrichment by immunoprecipitation (dsRIP)

Total RNAs were isolated by TRIzol, keeping samples at 4°C throughout the process to minimize complementary RNA annealing. TRIzol-isolated RNAs were diluted in ice-cold IP buffer (20 mM Tris-HCl [pH 7.4], 150 mM NaCl, 2 mM EDTA, 1% Nonidet P-40 (NP-40) (Sigma) and 100 U/mL RNaseOUT (Invitrogen)). The anti-dsRNA J2 antibody (English and Scientific Consulting Hungary, SCICONS) was combined to total RNAs derived from mock-, IIV-6- and DCV-infected S2 cells. RNA-J2 mixtures were incubated overnight at 4°C under rotation. Dynabeads Protein G (Invitrogen) were washed with IP buffer and combined with RNA-J2 mixture at 4°C for 4 h/rotating. Beads were captured in the magnetic stand and 5–8 times washed in IP buffer. RNAs associated to beads were extracted with TRIzol according to the manufacturer's recommendation.

DNase I treatment of RNA samples

Briefly, 0.4–10 μg of total RNAs extracted with TRIzol or from dsRIP samples were mixed to 5 μL of 10X buffer (100 mM Tris, pH 7.5, 25 mM $MgCl_2$, 5 mM $CaCl_2$), 2 U RNase-free DNase I (Invitrogen) and nuclease-free water up to 50 μL following incubation at 37°C/30 min. DNase I-treated RNAs were purified with Acid phenol-chloroform (Invitrogen).

RNA analysis: cDNA synthesis, PCR and qPCR reactions

DNase I-treated RNAs were quantified in Nanodrop (Thermo) and used in regular Reverse Transcription (RT) assays. Briefly, 400–1000 ng of RNAs were denatured at 70°C for 5 min and then reverse transcribed using Moloney murine leukaemia virus (M-MLV) reverse transcriptase. RT reactions without the reverse transcriptase (RT(−)) were performed as controls for genomic DNA contamination.

dsRNA precursors from IIV-6 Genomic regions 206R-209R and 224L-227L were detected using primers aligning to different genes/ORFs within individual regions. PCR assays were performed using DNA Taq polymerase (Invitrogen) and 100 nM of forward/reverse

primers. PCR cycling conditions: 95°C for 3 min; 35–40 cycles of 95°C for 30 s, 50°C for 30 s and 72°C for 60 s, and a single step at 72°C for 6 min. PCR reactions were mixed to 6X DNA loading buffer (Invitrogen) and then electrophoresed in 1–1.5% (wt/vol) agarose gels. PCR bands were analyzed by Sybr-safe (Invitrogen) or Ethidium Bromide staining and observed under the UV light.

Quantitative PCR (qPCR) reactions were performed using Power SYBR Master Mix (Applied Biosystems) and run on CFX384 Real-Time System (Bio-Rad) or QuantStudio 7 (Applied Biosystems) with the standard cycling programs for Cycle Threshold (Ct) and melting temperature (dissociation curve) analysis. Data were normalized by the *Drosophila* housekeeping Ribosomal protein L 32 (RpL32) or U6 RNA (under ActD and ML-60218 treatments) in case of cDNA using the delta Ct method for relative RNA quantifications. Isolated DNA from infected cells was resuspended in 200 μL of nuclease-free water and 5 μL were subjected to qPCR reactions for S2 and IIV-6 genomic DNA (gDNA) quantifications using delta Ct method and IIV-6 gDNA normalized by S2 DNA levels. Primers were designed using primer 3 plus tool (https://primer3plus.com/) and are described in Table S1.

Strand specific RT

Strand-specific RT (ssRT) assay was adapted from protocols introduced elsewhere (Peyrefitte et al., 2003; Plaskon et al., 2009). cDNA complementary to the target IIV-6 RNA sequence was synthesized with the specific primer including a 5′-tag unrelated to IIV-6 and *Drosophila* genomes (Plaskon et al., 2009). Briefly, 400–1000 ng of DNase I-treated, phenol purified RNAs were combined to 5′-tagged strand-specific primers at a final concentration of 0.2 μM, 4 μM dNTP mix (Thermo) in nuclease-free water. The mixture was incubated at 95°C for 5 min and 52°C for 2 min. The mix containing 12.5 ng/μL of ActD (Sigma), 2 U/μL RNaseOUT (Invitrogen), SuperScript III (SSPIII) buffer, 5 mM dithiothreitol and 10 U/μL of SSPIII in nuclease-free water was added to samples. ActD was used to inhibit the synthesis of the second cDNA strand (Perocchi et al., 2007). cDNA synthesis proceeded at 52°C for 55 min, and then SSPIII was inactivated at 75°C for 15 min. Unincorporated primers were removed using 2 U/μL of Exonuclease I mix (Thermo) at 37°C for 30 min and inactivated at 85°C for 5 min. PCR and qPCR assays were performed using the 5′-tag primer combined with the appropriate IIV-6–specific primer. For ssRT-PCR assays, we used proofreading Phusion (Thermo) or *Pfx* DNA polymerases (Invitrogen) for amplification. PCR bands were analyzed as described above. RNA levels were determined by the delta Ct method relative to 40 PCR cycles. Oligos were designed using primer 3 plus tool (https://primer3plus.com/) and are described in Table S1.

Small RNA sequencing

Small RNAs were size-selected (~18–29 nt) from the low molecular weight (LMW) RNA fractions on a denaturing PAGE essentially as described in (Pfeffer et al., 2004). Purified small RNA preparations from wildtype w[1118] flies injected with IIV-6 were used to construct small RNA libraries using SOLiD total RNA-seq kit (Ambion) and sequenced using the SOLiD platform (Applied Biosystems) at the Genomics Core of the Feinberg School of Medicine (Northwestern University). Libraries from size-selected small RNA preparations using control and Loqs-PD deficient flies infected with IIV-6 were constructed utilizing the TruSeq Small RNA Library Prep Kit (Illumina) according to vendor's protocol. Preparation of small RNA libraries from S2 cells were not size-selected, but an oligo that blocked cloning of 2 S rRNA was used instead (Wickersheim and Blumenstiel, 2013). Samples were sequenced on Illumina HiSeq2500 (flies) or HiSeq4000 (S2 cells) sequencers by IGBMC Sequencing Platform of Strasbourg/France. Details for sRNA-seq data from this study and public data are described in Table S2.

dsRNA immunoprecipitation (dsRIP) sequencing

Prior RNA-seq, dsRNAs were enriched in samples from IIV-6-infected cells. 24 μg of TRIzol-isolated total RNAs from mock- and IIV-6-infected samples were subjected to dsRIP, DNase I-treated (Ambion) and purified with Acid Phenol (Invitrogen). Then, libraries were cloned with the TruSeq Stranded Total RNA kit (Illumina), using the protocol recommended by the manufacturer. 2 × 100 nucleotides paired-end sequencing was performed on an Illumina HiSeq4000 sequencer by the IGBMC Sequencing Platform of Strasbourg/France (Strasbourg, France).

Analysis of small RNA sequencing datasets

Small RNA-seq analysis was performed essentially as described in (Aguiar et al., 2015) and consisted in (i) filtering reads by phred quality ≥20; (ii) adaptor trimming (Cutadapt v1.12) and exclusion of sequences shorter than 15 nt or containing ambiguous bases (Martin, 2011); (iii) Pre-processed read alignment to *Drosophila melanogaster* and IIV-6 reference genomes allowing 1 mismatch (Bowtie v1.1.2) (Langmead et al., 2009); (iv) exclusion of multi-aligned reads and sequences mapping to 2 S rRNA allowing 1 mismatch; (v) normalization of IIV-6 derived siRNAs (20–23 nt) by the total number of reads mapping to *D. melanogaster* genome (v6.09) and posterior representation as Reads per Million (RPM). For sRNA datasets from Control and *loqs-PD* deficient flies, IIV-6 derived reads were normalized either by total reads mapping to *D. melanogaster* genome (RPM) and by viral RNA loads (average of geometric means from IIV-6 MCP and 393L RNA levels). miRNAs and endo-siRNAs were normalized by total read mapping to *D. melanogaster* genome (RPM). siRNA derived from specific Transposon Elements were mapped to each reference (consensus) sequence with Bowtie allowing 1 mismatch. Analysis of small RNA size profile, 5′ base preference, density of coverage, and additional data analysis were evaluated using in-house Perl and R scripts. Intersection data were analyzed and plotted with Upset plot using an R package. The *D. melanogaster* (v6.09) genome and respective annotation were download from flybase.org and IIV-6 genome was download from NCBI. Calculation of the relationship among different sRNA-seq data from Illumina sequencing of IIV-6-infected flies and cells (Bronkhorst et al., 2012; Kemp et al., 2013), as well as SOLiD platform from this study (Table S2),

was performed dividing the IIV-6 genome into 8-bp bins that were used to determine the density profile for each library. Posteriorly, each library represented by a vector of bins was compared to each other by a distance-like metric represented as (1 – Pearson's correlation). Resulting distance matrix was used to hierarchically clustering of the samples using "UPGMA" as linkage method that was plotted in a dendrogram. The siRNA density was plotted against IIV-6 genome and visualized using Jbrowse (Buels et al., 2016). Hierarchical clustering was performed in R using built-in functions.

Definition of genomic regions enriched for siRNAs in the IIV6 genome

To define regions that presumably generate dsRNAs based on siRNA location, the density of siRNAs (the *n* times that a base was covered by any read) for each base of the IIV-6 reference genome was calculated and ranked in the different sRNA-seq datasets (Bronkhorst et al., 2012; Kemp et al., 2013 and SOLiD platform from this study). The top 5% densest bases (95% percentile) were select in each dataset independently of genomic annotation (gene/Intergenic region). To filter out for bases located in regions associated with high density of siRNAs in all datasets, only shared positions among the top 5% densest bases were retained and defined as siRNA hotspots. Hotspots were then associated with genes (ORFs) and Intergenic regions. Then, adjacent genes/intergenic regions containing hotspots were visually examined and sites with continuous coverage of siRNAs were merged into 14 genomic regions with high siRNA densities (hotspot-associated regions) that were separated by 14 hotspot depleted regions with discontinuous and low siRNA coverage. For each hotspot-associated or depleted region, the mean siRNA density (mean density of nucleotide coverage within the region) was calculated to generate a density map of the relative contribution of individual locations to total density (sum of the density means from hotspot-associated or depleted regions) in each dataset. To analyze enrichment of siRNAs within individual regions, the number of siRNAs arising from each region was calculated and compared to the expected number of siRNAs (mean coverage) covering the whole IIV-6 genome using Fisher's exact test. siRNA abundancies within hotspot-associated or depleted region were compared between Control and *loqs-PD* deficient flies using Pearson's correlation.

Density correlations between sRNA-seq and dsRIP-seq datasets

For dsRNA-seq analysis, paired-end reads were pre-processed using FASTX-Toolkit. Reads scored with phred quality below 20 were discarded (Gordon and Hannon, 2010). Filtered read pairs were merged into longer sequences using the PEAR program (Zhang et al., 2014). For transcription assessment, merged reads were compared against IIV-6 genome, genes (ORFs) and intergenic regions using Bowtie2 software and abundance separated by Left (L) and Right (R) genomic strands. For each position on the IIV-6 genome an R/L density value was attributed based on read coverages on each genomic strand. Using IIV-6 gene annotation, R/L density counts were redefined as sense/antisense according to the gene orientation. In this analysis, density counts from intergenic regions were removed, as sense/antisense directionalities could not be determined. The exception was the intergenic region 205R–206R that separates genomic region 205R from 206R to 209R, where reads mapping to R and L strands were considered sense and antisense, respectively. For downstream analysis, the density counts in sense/antisense orientations for genomic regions and inter-regions were calculated as the sum of densities of individual bases and normalized by the sum of gene lengths within each genomic region or inter-region to generate a density map of sense/antisense transcription. Then, sense/antisense transcription from dsRIP-seq was compared with siRNA density in genomic regions and inter-regions using Pearson's correlation. Details for RNA-seq data are described in Table S2.

Motif analysis

Putative conserved binding sites for transcription factors (Motifs) were predicted using MEME Suite with the variant MEME-CHIP setting the parameters known motifs to "*Drosophila melanogaster*", using "Combined *Drosophila* Databases" and expected motif distribution to "Any number of repetitions" (Bailey et al., 2015). Comparisons between the genomic position of motifs and hotspot-associated regions annotated in the IIV-6 genome, including Fisher's exact test for co-localization, were performed using flank, merge, fisher, reldist and closest programs built-in BEDTools package (Quinlan and Hall, 2010).

m^{6}A analysis

Data from m^{6}A methylation sites in *Drosophila melanogaster* was obtained from previously published datasets (Wang et al., 2021). Genomic positions of TEs or cis-NAT with methylation sites were compared using intersect program built-in BEDTools package. Abundance of TEs that co-localize with methylation sites was computed aligning small RNA reads against TE reference with Bowtie aligner allowing 1 mismatch, considering only 21-nt long reads normalized by Reads Per Million (RPM). To ascertain the origin, only single mapping small RNAs were considered. Odds ratio was computed using MedCalc (https://www.medcalc.org/). Statistics associated to proportion of elements within regions containing the m^{6}A modification was performed using built-in R Fisher's test with 105 Monte Carlo replicates. Differences in the abundance of 21-nt small RNAs derived from TEs within or outside regions with m^{6}A was assessed using two-sided Student's t-test.

Image processing

The images were first processed in Fiji (Schindelin et al., 2012). Briefly, raw Z-stacked images were open in ImageJ software, the separate channels were merged, and Z-Project was applied using Sum Slices or Average Intensity modes. The Scale bar was added, the images were flattened and all images from the same batch were combined in the same panel using Stack tools. Images were

saved in TIFF format and further processed in Photoshop (PS) where contrast and brightness were adjusted, and the final panels were assembled. Magnified views in insets (zooms) are shown as white boxes from the original images, that were further processed in PS. Scale bars were also adjusted according to magnification boxes in PS to keep zoom ratios. To analyze BrdU *foci* location related to nuclear DNA and/or dsRNA distribution, the images were split into separated channels and different slices merged using Z-Project tool. The Hoechst channel was used to analyze total DNA (cellular + viral DNA). An automatic threshold was applied to minimize noise while retaining most Hoechst signal. Hoechst areas were automatically selected in ImageJ Analyze Particles. The same procedure was applied to BrdU, Lamin0 and dsRNA channels. The resulting circularized areas were overlayed onto the multi-channel images (after applying Z-Project). When the analysis did not provide sufficiently stringent selection, a cut-off area was defined using ImageJ Analyze Particles for circularity selection. For cross-sections analysis, Multichannel Plot Profile from BAR tools (https://github.com/tferr/Scripts) in ImageJ was used in multi-channel composites to analyze the distribution of pixel intensities along a cross-section line. Airyscan images were analyzed using the Fiji plugin AiryscanJ (https://gitlab.inria.fr/serpico/airyscanj_bin) with pseudoconfocal processing.

QUANTIFICATION AND STATISTICAL ANALYSIS

Evaluation of statistical significance was performed using R scripts and GraphPad Prism software. We applied the Student *t*-test, One-way ANOVA with Dunnett's test or two-way ANOVA with Tukey's (comparing all means) or Sidak's test (comparing specific groups of means) to analyze statistically differences in DNA and RNA levels for qPCR assays as indicated in figure legends. For IIV-6 transcripts and replication analysis, data were log-transformed before statistical inference and plotted using non-transformed values. For bioinformatic analysis, statistical tests were described elsewhere (Aguiar et al., 2015; Marques et al., 2013). Correlation between dsRIP data and siRNAs were compared with Pearson's correlation. Fisher's exact test was used to evaluate Expected/Observed abundance of siRNAs from hotspots-associated versus depleted regions, the presence of motifs along IIV-6 genome and m^6A presence in host transcripts. Normality test for assessment of density of RNAs was performed using Shapiro's test. No statistical methods were used to pre-evaluate sample size.

Data and software availability

All the data are available from the authors upon request.